# Mathematical Aspects of Image Processing and Computer Vision 2003

Edited by Y. Giga, S. Izumiya, K. Deguchi

Sapporo, 2004

Series #81. March, 2004

Publication of this series is partly supported by Grant-in-Aid for formation of COE.

# HOKKAIDO UNIVERSITY
# TECHNICAL REPORT SERIES IN MATHEMATICS

#54 N. Kawazumi (Ed.), リーマン面に関連する位相幾何学, 122 pages. 1998.

#55 T. Ozawa and H.-F. Yamada (Eds.), 1997 年度談話会・特別講演アブストラクト集 Colloquium Lectures, 83 pages. 1998.

#56 Y. Giga, 界面ダイナミクス–曲率の効果, 講義録, 48 pages. 1998.

#57 J. Inoue (Ed.), 第 7 回関数空間セミナー報告集, 138 pages. 1999.

#58 Y. Giga and R. Kobayashi (Eds.), Abstracts of Sapporo Symposium on Anisotropic Effects in a Crystal Growth Problem and its Mathematical Analysis (SAM), 51 pages. 1999.

#59 Y. Giga and T. Ozawa (Eds.), Proceedings of thee 24th Sapporo Symposium on Partial Differential Equations, 61 pages. 1999.

#60 I. Tsuda and N. Kawazumi (Eds.), 1998 年度談話会・特別講演アブストラクト集, 55 pages. 1999.

#61 T. Ozawa (Ed.), Proceedings of Sapporo Guest House Minisymposium on Nonlinear Wave Equations, 67 pages. 1999.

#62 S. Miyajima, T. Takeo and J. Inoue (Eds.), 第 8 回関数空間セミナー報告集, 96 pages. 2000.

#63 K. Ono and N. Honda (Eds.), 1999 年度談話会・特別講演アブストラクト集, 43 pages. 2000.

#64 Y. Giga and T. Ozawa (Eds.), Proceedings of the 25th Sapporo Symposium on Partial Differential Equations, 55 pages. 2000.

#65 H. Nakamura (Ed.), ガロア・タイヒミュラー群の LEGO 理論, 37 pages. 2000.

#66 J. Inoue et al (Eds.), 関数空間セミナー報告集 2000, 134 pages. 2001.

#67 Y. Giga and H. Yamashita (Eds.), 2000 年度談話会・特別講演アブストラクト集, 61 pages. 2001.

#68 Y. Giga and T. Ozawa (Eds.), Proceedings of the 26th Sapporo Symposium on Partial Differential Equations, 67 pages. 2001.

#69 M. Matsumoto, 基本群へのガロア作用, 50 pages. 2001.

#70 T. Nakazi (Ed.), 第 10 回 関数空間セミナー報告集, 97 pages. 2002.

#71 Y. Giga (Ed.), Surface Evolution Equations - a level set method, 223 pages. 2002.

#72 T. Suwa and T. Yamanouchi (Eds.), 2001 年度談話会・特別講演アブストラクト集, 44 pages. 2002.

#73 T. Jimbo, T. Nakazi and M. Hayashi (Eds.), 第 11 回 関数空間セミナー報告集, 135 pages. 2003.

#74 T. Ozawa, Y. Giga, S. Jimbo and G. Nakamura (Eds.), Partial Differential Equations, 51 pages. 2002.

#75 D. Matsushita (Ed.), Proceedings of the workship "Hodge Theory and Algebraic Geometry", 191 pages. 2003.

#76 M. Hayashi and G. Ishikawa (Eds.), 2002 年度談話会・特別講演アブストラクト集, 34 pages. 2003.

#77 T. Ozawa, Y. Giga, S. Jimbo, K. Tsutaya, Y. Tonegawa and G. Nakamura(Eds.), Proceedings of the 28th Sapporo Symposium on Partial Differential Equations, 76 pages. 2003.

#78 S. Izumiya, G. Ishikawa, T. Sano and I. Shimada (Eds.), The 12th MSJ-IRI "Singularity Theory and Its Applications" ABSTRACTS, 291 pages. 2003.

#79 H. Kubo and T. Ozawa (Eds.), Proceedings of Sapporo Guest House Symposium on Mathematics 15 "Evolution Equations", 31 pages. 2003.

#80 S. Miyajima, F. Takeo and T. Nakazi (Eds.), 第 1 2 回関数空間セミナー報告集, 122 pages. 2004.

# Mathematical Aspects of Image Processing and Computer Vision 2003

Edited by Y. Giga, S. Izumiya, K. Deguchi

Sapporo, 2004

Partly supported by the Grast-in-Aid for Scientific Research, No. 14204011, the Japan Society of the Promotion of Science

Co-sponsor : Graduate School of Information Sciences, Tohoku University

# PREFACE

In the year 2000 we began to organize a symposium on mathematical aspects of image processing and computer vision so that mathematicians and engneering people have chances to discuss common topics and work together from different points of view.

This meeting is the fourth one and is attracting more people than we expected.

We take this opportunity to publish abstracts of lectures. We hope this is helpful for many people who are potentially interested in the topics.

Finally, I thank Professor Koichiro Deguchi and Professor Shyuichi Izumiya who coorganized this meeting.

Sapporo
March 2004

Yoshikazu Giga

# CONTENTS

## Programme

as of October 29, 2003

# Mathematical Center for Advanced Study Symposium Sapporo Guest House Symposium on Mathematics 16

## *Mathematical Aspects of Image Processing and Computer Vision 2003*

Organizers: Y. Giga (Hokkaido U.)
S. Izumiya (Hokkaido U.)
K. Deguchi (Tohoku U.)

November 27, 2003 (Thursday) (Venue : Room 3-512, Dept. of Math.)

14:00–15:00 ARAI, Hitoshi (U. Tokyo) (新井仁之, 東大数理)
Visual Perception and Nonlinear Information Processing based on Wavelets

15:30–16:30 KASHIMA, Yohei (U. Sussex/Hokkaido. U)(鹿島洋平, サセックス大/北大)
A mathematical solvability for the denoising of a singular color image model (joint work with N. Yamazaki and Y. Giga)

November 28, 2003 (Friday) (Venue : Room 3-508/512, Dept. of Math.)

10:00–11:00 TOKUYAMA, Takeshi (Tohoku U.)(徳山豪, 東北大情報)
Digital Halftoning and Global Roundings of Graphs and Hypergraphs

11:30–12:30 KIMIA, Benjamin B. (Brown Univ.)
On the Local Form and Transitions of the Medial Axis/ Shock Graph and Their Role in Object Recognition

14:30–15:30 TSAI, Y. -H. Richard (Princeton Univ.)
Dynamic Visibility in a PDE based Implicit Framework

16:00–16:40 TORII, Akihiko (Chiba U.)(鳥居秋彦, 千葉大)
Linear and Nonlinear Subpixel Superresolution Techniques (joint work with A. Imiya)

18:00 Welcome Party

November 29, 2003 (Saturday) (Venue : Sapporo Guest House)

10:00–11:00 SANO, Takashi (Hokkai-Gakuen U.)(佐野貴志, 北海学園大)
Generic Centro-affine Differential Geometry of Curves

11:30–12:30 DEGUCHI, Kohichiro (Tohoku U.)(出口光一郎, 東北大情報)
A Theory of Negative Shape : Revisited
(joint work with P. Ghosh)

Venues :
- November 27, Room 3-512 (Fifth floor of building # 3, Faculty of Science, Hokkaido U.)
- November 28, Room 3-508/512 (Fifth floor of building # 3, Faculty of Science, Hokkaido U.)
- November 29, Sapporo Guest House, 8 minute walk from Sumikawa Subway Station

Sapporo Guest House : 1-80, 2-jo 17-chome, Hiragishi, Toyohira-ku Sapporo, 062-0932 Japan
札幌天神山国際ハウス: 札幌市豊平区平岸２条１７丁目 1-80

TEL (011)823-1000 FAX (011)823-1867

Secretariat : Ms. Ayako Kanayama TEL/FAX: 011-706-4839
e-mail: gjr@math.sci.hokudai.ac.jp

# Visual Perception and Nonlinear Information Processing based on Wavelets

Hitoshi ARAI
The University of Tokyo
E-mail address : h-arai@ms.u-tokyo.ac.jp

## Abstract

This talk is concerned with image processing in the visual system related to visual illusions. As known, it is widely believed that visual illusions will offer us a clue to understand how our visual system carries out information processing. From this reason, over the past 100 years, many studies have been made on the mechanisms of occurrence of visual illusions.

So far, in order to study visual illusions, many researchers used psychological methods, neuroscience, neural networks or filtering, etc.

In this talk, we design a computational system modeled after some functions of striate cortex in human's brain by employing both the maximal overlap multiresolution analysis with respect to a biorthogonal wavelet and some new nonlinear processing. We show several computer simulations obtained by this system. From these simulations we explain in terms of mathematics the mechanism of occurrence of several visual illusions which are produced by information processing in the pathway from the retina to the striate cortex.

# A MATHEMATICAL SOLVABILITY FOR THE DENOISING OF A SINGULAR COLOR IMAGE MODEL

YOSHIKAZU GIGA
Department of Mathematics, Hokkaido University, Sapporo 060-0810, Japan
E-mail: giga@math.sci.hokudai.ac.jp

YOHEI KASHIMA
Department of Mathematics, University of Sussex, Brighton BN1 9QH, UK
E-mail: y.kashima@sussex.ac.uk
/ Department of Mathematics, Hokkaido University, Sapporo 060-0810, Japan

NORIAKI YAMAZAKI
Department of Mathematical Science, Common Subject Division, Muroran Institute of Technology, 27-1 Mizumoto-cho, Muroran, 050-8585, Japan
E-mail: noriaki@mmm.muroran-it.ac.jp

## 1 Introduction

As one denoising process in color image, we can consider a couple of diffusion flow equations for brightness and chromaticity of the color data. If we denote $v : \Omega(\subset \mathbb{R}^2) \to \mathbb{R}^N$ as a color image, then its brightness and its chromaticity at each pixel are given by the magnitude $M(x) := |v(x)|$ and the unit vector $u(x) := v(x)/M(x)$ respectively. While the magnitude diffusion for scaled $M(x,t)$ is described by gradient flow equations for a scalar valued function, the chromaticity diffusion for scaled $u(x,t)$ is proposed as constrained gradient system for a vector valued (more generally manifold valued) function (see [8]). In this work we are especially concerned with a solvability of the denoising process for the chromaticity $u(x,t)$ preserving chroma discontinuities and its length $|u(x,t)| = 1$.

The problem we are concerned with can be written as

$$u_t(x,t) = -\pi_{u(x,t)}\left(-\operatorname{div}\left(\frac{\nabla u(x,t)}{|\nabla u(x,t)|}\right)\right),$$

where the map $\pi_{u(x,t)}(\cdot)$ denotes the orthogonal projection from $\mathbb{R}^N$ to the tangent space of the unit sphere $S^{N-1}$ at $u(x,t)$. Since the projection $\pi_{u(x,t)}(\cdot)$ has the precise form of $\pi_u(w) = w - \langle w, u\rangle u$ and now $|u(x,t)| = 1$, our problem is equivalent to

$$u_t(x,t) = \operatorname{div}\left(\frac{\nabla u(x,t)}{|\nabla u(x,t)|}\right) + |\nabla u(x,t)|u(x,t).$$

The first difficulty to show its solvability is that this equation has strong singularity at points where $|\nabla u(x,t)| = 0$. This equation is derived by an energy functional of total variation of $u$, $\int_\Omega |\nabla u| dx$, in order to preserve the edge discontinuity of chromaticity of the original image. Therefore we need to formulate the problem mathematically. We formulate our problem by using subdifferential, which is an extended notion of differential, of the energy function of total variation. The second difficulty is that the problem does not have simple variational structure as a gradient flow equation due to the last term $|\nabla u(x,t)|u(x,t)$ which must be put to constrain the length of $u$ to be always 1. Therefore, the general framework for solvability by nonlinear semigroup theory does not work in our case. We will establish new mathematical framework to attain our purpose.

Roughly speaking our framework asserts that if some energy functionals approximate our energy of total variation in the sense of Mosco, solutions solving the corresponding problems derived by the approximate energies also converge to a solution of our original problem.

Practically it is possible to show that $p-$energy functional $\phi_p(u)$ $(p > 1)$

$$\phi_p(u) = \frac{1}{p} \int_\Omega |\nabla u(x)|^p dx$$

converges to our energy functional $\phi(u) = \int_\Omega |\nabla u(x)| dx$ of total variation of $u$ in the sense of Mosco. Thus, by applying this new framework to $p-$harmonic map flow equation

$$u_t(x,t) = -\pi_{u(x,t)} \left( -\operatorname{div} \left( |\nabla u(x,t)|^{p-2} \nabla u(x,t) \right) \right) \quad (p > 1)$$

for which some solvability results are known at present (see [3]), we show the existence of local in time solution of our problem for a general target manifold and a smooth initial data with small energy.

## 2 Subdifferential formulation

We always assume periodic boundary condition; all the functions are now supposed to be defined on $\mathbb{T}^n := \prod_{i=1}^n (\mathbb{R}/\omega_i \mathbb{Z})$ for given $\omega_i > 0$ $(i = 1, 2, \cdots, n)$. Note that the formulation for the case with Dirichlet boundary condition can be done by the similar way. We consider the general case that the target manifold is not only the unit sphere $S^{N-1}$ but also any compact manifold $M$ ( without boundary ) smoothly embedded in $\mathbb{R}^N$. The initial value problem we are going to formulate is

$$\begin{cases} u_t = -\pi_u \left( -\operatorname{div} \left( \dfrac{\nabla u}{|\nabla u|} \right) \right) & \text{in } \mathbb{T}^n \times (0,T], \\ u = u_0 & \text{on } \mathbb{T}^n \times \{0\}, \end{cases} \tag{EQ}$$

where $\pi_u$ denotes the orthogonal projection from $\mathbb{R}^N$ to the tangent space $T_u M$ of $M$ at $u$ and the initial data $u_0$ is a map from $\mathbb{T}^n$ to $M$.

To formulate this problem as an evolution equation in $L^2(0,T; L^2(\mathbb{T}^n, \mathbb{R}^N))$ next we define the energy functional of total variation as a functional on $L^2(\mathbb{T}^n, \mathbb{R}^N))$.

$$\phi(u) := \begin{cases} \displaystyle\int_{\mathbb{T}^n} |\nabla u(x)| dx & \text{if } u \in BV(\mathbb{T}^n, \mathbb{R}^N) \cap L^2(\mathbb{T}^n, \mathbb{R}^N), \\ +\infty & \text{otherwise,} \end{cases}$$

where $BV(\mathbb{T}^n, \mathbb{R}^N)$ denotes the space of functions of bounded variation on $\mathbb{T}^n$ with values in $\mathbb{R}^N$. Moreover, we define the energy $\Phi^T$ on $L^2(0,T;L^2(\mathbb{T}^n,\mathbb{R}^N))$ by $\Phi^T(u) := \int_0^T \phi(u(t))dt$.

To complete the formulation we need to prepare several other notations. Let $L^2(\mathbb{T}^n, M)$ denote the closed subset of $L^2(\mathbb{T}^n,\mathbb{R}^N)$ defined by $L^2(\mathbb{T}^n, M) := \{u \in L^2(\mathbb{T}^n,\mathbb{R}^N) \mid u(x) \in M \text{ a.e. } x \in \mathbb{T}^n\}$. Let $L^2(0,T;L^2(\mathbb{T}^n, M))$ denote the set of all $L^2$-mappings from $[0,T]$ to $L^2(\mathbb{T}^n, M)$. For any $g \in L^2(0,T;L^2(\mathbb{T}^n, M))$ we define a map $P_g(\cdot) : L^2(0,T;L^2(\mathbb{T}^n,\mathbb{R}^N)) \to L^2(0,T;L^2(\mathbb{T}^n,\mathbb{R}^N))$ by

$$P_g(f)(x,t) = \pi_{g(x,t)}(f(x,t)) \text{ for a.e. } (x,t) \in \mathbb{T}^n \times [0,T]$$

for any $f \in L^2(0,T;L^2(\mathbb{T}^n,\mathbb{R}^N))$.

If we formally calculate the variational derivative of $\Phi^T$, which is denoted by $\delta\Phi^T(u)/\delta u$, we see that

$$\frac{\delta\Phi^T}{\delta u}(u) = -\operatorname{div}\left(\frac{\nabla u}{|\nabla u|}\right) \text{ in } L^2(0,T;L^2(\mathbb{T}^n,\mathbb{R}^N)).$$

Therefore we can think of our problem as an evolution problem in $L^2(0,T;L^2(\mathbb{T}^n,\mathbb{R}^N))$.

$$\begin{cases} u_t = -P_u\left(\dfrac{\delta\Phi^T}{\delta u}(u)\right) & \text{in } L^2(0,T;L^2(\mathbb{T}^n,\mathbb{R}^N)), \\ u|_{t=0} = u_0 & \text{in } L^2(\mathbb{T}^n, M). \end{cases}$$

The term $\delta\Phi^T(u)/\delta u$, however, does not have a rigorous mathematical meaning. In order to formulate the derivative of such a singular energy we use the notion of subdifferential. We define the subdifferential operator $\partial\Phi^T(u)$ of our energy $\partial\Phi^T$ as

$$\partial\Phi^T(u) := \{\, v \in L^2(0,T;L^2(\mathbb{T}^n,\mathbb{R}^N)) \mid \Phi^T(u+h) \geq \Phi^T(u) + \langle v, h\rangle_{L^2(0,T;L^2(\mathbb{T}^n,\mathbb{R}^N))} \text{ for any } h \in L^2(0,T;L^2(\mathbb{T}^n,\mathbb{R}^N)) \,\}.$$

Although subdifferential of a convex funtional is multi-valued operator in general, it is known that the value of the subdifferental is equal to the derivative of the energy where it is differentiable. Therefore we can think that subdifferential is a natural extension of differential. By using $\partial\Phi^T$ we complete the mathematical formulation of our singular problem as

$$\begin{cases} u_t \in -P_u\left(\partial\Phi^T(u)\right) & \text{in } L^2(0,T;L^2(\mathbb{T}^n,\mathbb{R}^N)), \\ u|_{t=0} = u_0 & \text{in } L^2(\mathbb{T}^n, M). \end{cases} \tag{EQ1}$$

Now we can define the solution of our problem.

**Definition 2.1.** We call a function $u : \mathbb{T}^n \times [0,T] \to \mathbb{R}$ is a solution of (EQ) if $u$ belongs to $L^2(0,T;L^2(\mathbb{T}^n,\mathbb{R}^N)) \cap C([0,T],L^2(\mathbb{T}^n,\mathbb{R}^N))$ and satisfies (EQ1).

# 3 Convergence properties

We derive some convergence properties for convex energy and set of $L^2$ space, which are used to establish our framework. We approximate the right hand side $P_u(\partial\Phi^T(u))$ of our problem by the right hand side of $p-$harmonic flow equation. Let us define $p-$energy first in our setting.

$$\phi_m(u) := \begin{cases} \frac{1}{1+1/m}\int_{\mathbb{T}^n} |\nabla u(x)|^{1+1/m} dx & \text{if } u \in W^{1,1+1/m}(\mathbb{T}^n, \mathbb{R}^N) \cap L^2(\mathbb{T}^n, \mathbb{R}^N), \\ +\infty & \text{otherwise,} \end{cases}$$

for $m = 1, 2, \cdots$. Again by using this $\phi_m$ we define $\Phi_m^T$ by $\Phi_m^T(u) := \int_0^T \phi_m(u(t))dt$ as a convex functional on $L^2(0,T; L^2(\mathbb{T}^n, \mathbb{R}^N))$. Under these notations $p-$harmonic map flow equation can be written as

$$\begin{cases} u_t \in -P_u(\partial\Phi_m^T(u)) & \text{in } L^2(0,T; L^2(\mathbb{T}^n, \mathbb{R}^N)), \\ u|_{t=0} = u_0 & \text{in } L^2(\mathbb{T}^n, M). \end{cases}$$

As the first convergence we have

**Proposition 3.1.** *(see [7]) The functional $\phi_m$ converges to $\phi$ in the sense of Mosco as $m \to +\infty$, i.e.,*

*(i) If $v_m \rightharpoonup v$ weakly in $L^2(\mathbb{T}^n, \mathbb{R}^N)$, then $\phi(v) \le \liminf_{m\to+\infty} \phi_m(v_m)$ holds.*

*(ii) For any $v \in D(\phi)$ there exists $v_m \in L^2(\mathbb{T}^n, \mathbb{R}^N)$ such that $v_m \to v$ strongly in $L^2(\mathbb{T}^n, \mathbb{R}^N)$ and $\lim_{m\to+\infty} \phi_m(v_m) = \phi(v)$.*

Then by applying the general theory developed in [1] or [6] to the Mosco convergence $\phi_m \to \phi$, we can obtain

**Proposition 3.2.** *The functional $\Phi_m^T$ converges to $\Phi^T$ in the sense of Mosco as $m \to +\infty$.*

Moreover the Mosco convergence above yields (see [2])

**Proposition 3.3.** *The subdifferential operator $\partial\Phi_m^T$ converges to $\partial\Phi^T$ in the sense of Graph, i.e.,*

*for any $(u, v) \in \Phi^T$ there exists $(u_m, v_m) \in \Phi_m^T$ such that $u_m \to u$ and $v_m \to v$ strongly in $L^2(0,T; L^2(\mathbb{T}^n, \mathbb{R}^N))$ as $m \to +\infty$.*

In addition we introduce a notion of convergence of set. We define *sequentially weak upper limit* of a sequence $\{S_m\}_{m=1}^{+\infty}$ of subset of a real Hilbert space $H$ denoted by $\mathrm{sqw} - \mathrm{Limsup}_{m\to+\infty} S_m$ as follows.

$$\underset{m\to+\infty}{\mathrm{sqw} - \mathrm{Limsup}}\, S_m := \{x \in H \mid \text{there exist } \{m_k\}_{k=1}^{+\infty} \subset \mathbb{N} \text{ and } x_k \in S_{m_k}\ (k = 1, 2, \cdots)$$
$$\text{such that } x_k \rightharpoonup x \text{ weakly in } H \text{ as } k \to +\infty\}.$$

Then in our case we observe that

**Proposition 3.4.** *Assume that $u_m$ converges to $u$ strongly in $L^2(0,T;L^2(\mathbb{T}^n,\mathbb{R}^N))$ and $\partial\Phi_m^T(u_m) \neq \emptyset$ $(m=1,2,\cdots)$. Then*

$$\operatorname*{sqw-Limsup}_{m\to+\infty} \partial\Phi_m^T(u_m) \subset \Phi^T(u).$$

We finally want to put the projection $P_u$ in front of the subdifferential operator in the above inclusion.

**Proposition 3.5.** *Let $\{u_m\}_{m=1}^{+\infty} \subset L^2(0,T;L^2(\mathbb{T}^n,M))$ converge to $u$ in $L^2(0,T;L^2(\mathbb{T}^n,\mathbb{R}^N))$ strongly and satisfy $\partial\Phi_m^T(u_m) \cap B_R \neq \emptyset$ $(m=1,2,\cdots)$ for a closed ball $B_R$ in $L^2(0,T;L^2(\mathbb{T}^n,\mathbb{R}^N))$ defined by*

$$B_R := \{u \in L^2(0,T;L^2(\mathbb{T}^n,\mathbb{R}^N)) \mid \|u\|_{L^2(0,T;L^2(\mathbb{T}^n,\mathbb{R}^N))} \leq R\}.$$

*Then we see*

$$\operatorname*{sqw-Limsup}_{m\to+\infty} P_{u_m}(\partial\Phi_m^T(u_m) \cap B_R) \subset P_u(\partial\Phi^T(u)).$$

Now we are ready to state our framework.

**Theorem 3.6 (Convergence theorem).** *Assume that $u_m \in L^2(0,T;L^2(\mathbb{T}^n,\mathbb{R}^N))$ $(m=1,2,\cdots)$ satisfies*

$$\begin{cases} u_{m,t} \in -P_{u_m}(\partial\Phi_m^T(u_m) \cap B_R) & \text{in } L^2(0,T;L^2(\mathbb{T}^n,\mathbb{R}^N)), \\ u_m|_{t=0} = u_{0,m} & \text{in } L^2(\mathbb{T}^n,M) \end{cases}$$

*with $R>0$ independent of $m$, where $u_{0,m} \in L^2(\mathbb{T}^n,M)$. Moreover, assume that*

$$\begin{aligned} &u_{0,m} \to u_0 \text{ strongly in } L^2(\mathbb{T}^n,\mathbb{R}^N) \text{ as } m\to+\infty, \text{ and} \\ &\limsup_{m\to+\infty} \phi_m(u_{0,m}) \leq \phi(u_0). \end{aligned}$$

*Then, there exists a function $u \in C([0,T],L^2(\mathbb{T}^n,\mathbb{R}^N))$ such that*

$$\begin{cases} u_t \in -P_u\left(\partial\Phi^T(u)\right) & \text{in } L^2(0,T;L^2(\mathbb{T}^n,\mathbb{R}^N)), \\ u|_{t=0} = u_0 & \text{in } L^2(\mathbb{T}^n,M), \end{cases}$$

*and $u$ satisfies the energy equality*

$$\int_0^t \int_{\mathbb{T}^n} |u_t(x,\tau)|^2 dx d\tau + \phi(u(t)) = \phi(u_0) \text{ for any } t \in [0,T].$$

*This means that $u$ is a solution of (EQ) in the sense of Definition 2.1.*

Note that the strong convergence of $u_m$ to $u$ can be proved by combining the energy equality

$$\int_0^t \int_{\mathbb{T}^n} |u_{m,t}(x,\tau)|^2 dx d\tau + \phi_m(u_m(t)) = \phi_m(u_{m,0}) \text{ for any } t \in [0,T],$$

with Ascoli-Arzela's theorem (for $C([0,T],L^2(\mathbb{T}^n,\mathbb{R}^N))$ ).

# 4 Solvability result

We assumed the solvability of $p-$harmonic map flow equation and the condition that $\partial\Phi_m^T(u_m) \subset B_R$ $(m = 1, 2, \cdots)$ for the solution $u_m$ of $p-$harmonic map flow equation in Convergence theorem. If we examine the latest solvability result of $p-$harmonic map flow equation [3], we observe that these conditions are satisfied in a local time. Therefore as an application of Convergence theorem we obtain the following local solvability theorem.

**Theorem 4.1 (Local Existence theorem).** *For any $K > 0$ there exists $\varepsilon_0 > 0$ depending only on $\mathbb{T}^n, M$, and $K$ such that if the initial data $u_0 : \mathbb{T}^n \to M$ satisfies following conditions;*

*(i)* $u_0 \in C^{2+\alpha}(\mathbb{T}^n, \mathbb{R}^N)$ $(0 < \alpha < 1)$,

*(ii)* $\|\nabla u_0\|_{L^\infty(\mathbb{T}^n)} \leq K$,

*(iii) there exists* $m_0 \in \mathbb{N}, \geq 3$ *such that*

$$\phi_{m_0}(u_0) + \frac{1}{m_0 + 1} \prod_{i=1}^{n} \omega_i \leq \varepsilon_0.$$

*Then, for any* $T \in \left(0, \dfrac{2}{C\sqrt{max\{1, K^2\}}}\right)$ *where $C$ is a positive constant depending only on $M$, there exists a function $u \in C([0,T], L^2(\mathbb{T}^n, M))$ solving (EQ) for this $T$ in the sense of Definition 2.1 and satisfying the energy equality*

$$\int_0^t \int_{\mathbb{T}^n} |u_t(x,\tau)|^2 dx d\tau + \phi(u(t)) = \phi(u_0) \text{ for any } t \in [0,T].$$

# References


[1] H. Attouch, *Convergence de functionnelles convexes*, Journes d'Analyse Non Linaire, Proc.Conf., Besan on(1977),1-40, Lecture Notes in Math.,665,Springer,Berlin(1978).

[2] H. Attouch, *Variational Convergence for Functions and Operators*, Pitman Advanced Publishing Program, Boston-London-Melbourne(1984).

[3] A. Fardoun and R. Regbaoui, *Heat flow for p−harmonic maps with small initial data*, Calc. Var. Partial Differential Equations.,16(2003),1-16.

[4] Y. Giga, Y. Kashima and N. Yamazaki, *Local solvability of a constrained gradient system of total variation*, Abstract and Applied Analysis, to appear.

[5] Y. Giga and R. Kobayashi, *On constrained equations with singular diffusivity*, Methods. Appl. Anal., to appear.

[6] N. Kenmochi, *Solvability of Nonlinear Evolution Equations with Time-Dependent Constraints and Applications*, The Bulletin of The Faculty of Education, Chiba University, 30(1981).

[7] K. Shirakawa, *Asymptotic convergence of p−Laplace equations with constraint as p tends to 1*, Math. Methods. Appl. Sci. 25(2002),No.9,771-793.

[8] B. Tang, G. Sapiro and V. Caselles, *Color image enhancement via chromaticity diffusion*, IEEE Transactions on Image Processing, 10(No.5)(2001),701-707.

# Digital Halftoning and Global Roundings of Graphs and Hypergraphs

Takeshi Tokuyama( Tohoku U.)

**Abstract**

Given a connected weighted graph $G = (V, E)$, we consider a hypergraph $H_G = (V, \mathcal{P}_G)$ corresponding to the set of all shortest paths in $G$. For a given real assignment $\mathbf{a}$ on $V$ satisfying $0 \leq \mathbf{a}(v) \leq 1$, a global rounding $\alpha$ with respect to $H_G$ is a binary assignment satisfying that $|\sum_{v \in F} \mathbf{a}(v) - \alpha(v)| < 1$ for every $F \in \mathcal{P}_G$. We conjecture that there are at most $|V|+1$ global roundings for $H_G$, and also the set of global roundings is an affine independent set. We give several positive evidences for the conjecture. We also show application of global roundings to digital halftoning. This abstract is based on a series of joint papers with T. Aasno, N. Katoh, H. Tamaki, N. Takki-Chebihi, and others.

## 1 Introduction

Given a real number $a$, an integer $k$ is a *rounding* of $a$ if the difference between $a$ and $k$ is strictly less than 1, or equivalently, if $k$ is the floor $\lfloor a \rfloor$ or the ceiling $\lceil a \rceil$ of $a$. We extend this usual notion of rounding into that of *global rounding* on hypergraphs as follows.

Let $H = (V, \mathcal{F})$, where $\mathcal{F} \subset 2^V$, be a hypergraph on a set $V$ of $n$ nodes. Given a real valued function $\mathbf{a}$ on $V$, we say that an integer valued function $\alpha$ on $V$ is a *global rounding* of $\mathbf{a}$ with respect to $H$, if $w_F(\alpha)$ is a rounding of $w_F(\mathbf{a})$ for each $F \in \mathcal{F}$, where $w_F(f)$ denotes $\sum_{v \in F} f(v)$. We assume in this paper that the hypergraph contains all the singleton sets as hyperedges; thus, $\alpha(v)$ is a rounding of $\mathbf{a}(v)$ for each $v$, and we can restrict our attention to the case where the ranges of $\mathbf{a}$ and $\alpha$ are $[0, 1]$ and $\{0, 1\}$ respectively.

This notion of global roundings on hypergraphs is closely related to that of *discrepancy* of hypergraphs[5, 4]. Given $\mathbf{a}$ and $\mathbf{b} \in [0, 1]^V$, define the *discrepancy* $D_H(\mathbf{a}, \mathbf{b})$ between them on $H$ by

$$D_H(\mathbf{a}, \mathbf{b}) = \max_{F \in \mathcal{F}} |w_F(\mathbf{a}) - w_F(\mathbf{b})|.$$

The supremum $\sup_{\mathbf{a} \in [0,1]^V} \min_{\alpha \in \{0,1\}^V} D_H(\mathbf{a}, \alpha)$ is called the linear (or inhomogeneous) discrepancy of $H$, and it is a quality measure of approximability of a real vector with an integral vector to satisfy constraints given by the linear system corresponding to $H$.

Thus, the set of global roundings of $\mathbf{a}$ is the set of integral points in the open unit ball around $\mathbf{a}$ where the distance is measured by the discrepancy $D_H$. It is known that the open ball always contains an integral point for any "input" $\mathbf{a}$ if and only if the hypergraph is unimodular (see [4]). This fact is utilized in digital halftoning applications [1, 2]. It is NP-hard to decide whether the ball is empty (i.e. containing no integral point) or not even for some very simple hypergraphs [3].

In this paper, we are interested in the maximum number $\nu(H)$ of integral points in an open unit ball under the discrepancy distance.

This direction of research is initiated by Sadakane *et al.*[6] where the authors discovered a surprising fact that $\nu(I_n) \leq n+1$ where $I_n$ is a hypergraph on $V = \{1, 2, .., n\}$ with edge set $\{[i, j]; 1 \leq i \leq j \leq n\}$ consisting of all subintervals of $V$. We can also see that $\nu(H) \geq n+1$ for any hypergraph $H$: if we let $\mathbf{a}(v) = \epsilon$ for every $v$, where $\epsilon < 1/n$, then any binary assignment on $V$ that assigns 1 to at most one vertex is a global rounding of $H$, and hence $\nu(H) \geq n+1$.

Given this discovery, it is natural to ask for which class of hypergraphs this property $\nu(H) = n+1$ holds. The understanding of such classes may well be related to algorithmic questions mentioned above. In fact, Sadakane *et al.* give an efficient algorithm to enumerate all the global roundings of a given input on $I_n$.

In this paper, we show that $\nu(H) = n+1$ holds for a considerably wider class of hypergraphs. Given a connected $G$ in which edges are possibly weighted by a positive value, we define a *shortest-path hypergraph* $H_G$ generated by $G$ as follows: a set $F$ of vertices of $G$ is an edge of $H_G$ if and only if $F$ is the set of vertices of some shortest path[1] in $G$ with respect to the given edge weights. In this notation, $I_n = H_{P_n}$ for the path $P_n$ on $n$ vertices. Note that we permit more than one shortest path between a pair of nodes if they have the same weight. We give several basic properties of the structure of a set of global roundings for $H_G$, and prove the following theorem:

**Theorem 1.1** *$\nu(H_G) = n+1$ holds for the shortest-path hypergraph $H_G$, if $G$ is an outerplanar graph, an unweighted mesh, or an unweighted $k$-tree.*

Based on the positive evidence above and some failed attempts in creating counterexamples, we conjecture that the result holds for general connected graphs.

**Conjecture 1.2** *$\nu(H_G) = n+1$ for any connected graph $G$ with $n$ nodes.*

## References


[1] T. Asano, N. Katoh, K. Obokata, and T. Tokuyama, Matrix Rounding under the $L_p$-Discrepancy Measure and Its Application to Digital Halftoning, SIAM J. Comput, 32(6) 14223-1435, 2003.

[2] T. Asano, T. Matsui, and T. Tokuyama, Optimal Roundings of Sequences and Matrices, *Nordic Journal of Computing* 7, 2000, pp.241-256.

[3] T. Asano and T. Tokuyama, How to Color a Checkerboard with a Given Distribution – Matrix Rounding Achieving Low $2 \times 2$ Discrepancy, *Proc. ISAAC2001* LNCS 2223, 2001, pp. 636-648.

[4] J. Beck and V. T. Sós, *Discrepancy Theory*, ine T. Graham, M. Grötshel, and L. Lovász (Eds.) *Handbook of Combinatorics,* Vol. II, Elsevier Sciences, 1995, Chapter 26, pp. 1405-1446.

[5] B. Chazelle, *The Discrepancy Method: Randomness and Complexity*, Princeton University Press, 2000.


[1] Precisely speaking, minimum weight path

[6] K. Sadakane, N. Takki-Chebihi, and T. Tokuyama, Combinatorics and Algorithms on Low-Discrepancy Roundings of a Real Sequence, *Proc. ICALP2001,* LNCS 2076, 2001, pp. 166-177.

[7] N. Takki-Chebihi and T. Tokuyama, Enumerating Global Roundings of an outerplanar graph, *to appear in Proc. ISAAC2003*, 2003.

# On the Local Form and Transitions of the Medial Axis/Shock Graph and Their Role in Object Recognition

Benjamin B. Kimia
Brown University

Nov 28, 2003

Presented at the "Mathematical Aspects of Image processing and Computer Vision 2003 (MCAS'03)
SAPPORO, JAPAN

# Shape Representation and Recognition

## 1. Generic Object Recognition: 2D Shape

A. Recognition via shock–graph edit distance **(ICCV `01, PAMI `04, SODA `00, SODA `01, IJCV `03-1, IJCV `03-2)**
   - Requires robustness against visual transformations
   - Dynamic Representation of shape as a point in a continuous deformation space (**shape space**)
   - Shape ⇔ **Shock graph** (Medial axis geometry plus a notion of dynamics of flow)
   - **Too many paths:** Equivalence class using instabilities or transitions of the shock-graph.
   - **Similarity** is the "cost" of least action path between two shapes
   - **Edit Distance** is used to find the optimal path in polynomial time
   - Databases: 32, 99, 216, 384 (**100% Recognition** in top three)

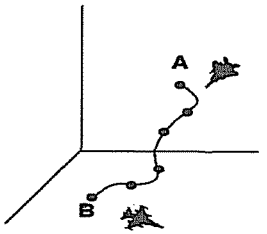


**Shape Space**

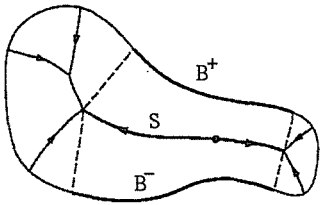


**Shock Graph**

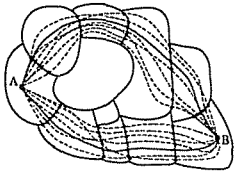


**Bundled Deformation Paths**

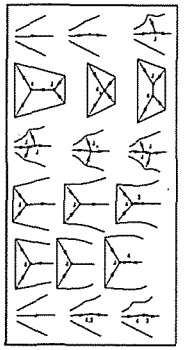

**Shock Transitions**

**Boundary Noise**

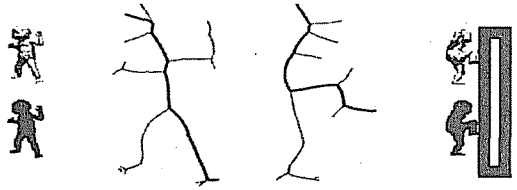

**Articulation/Viewpoint Variation**

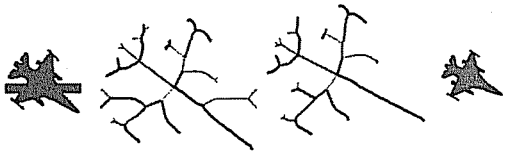

**Partial Occlusion**

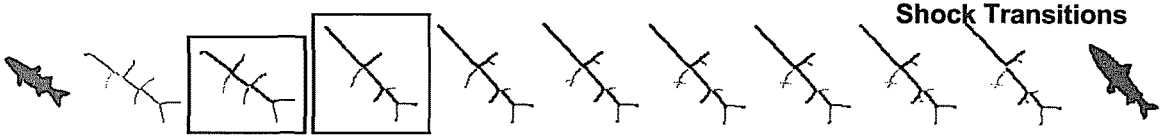

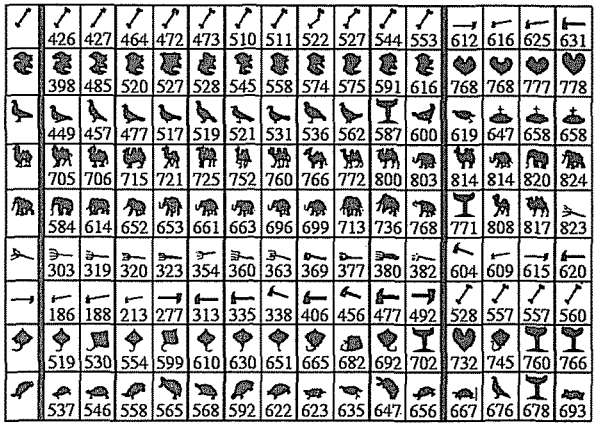


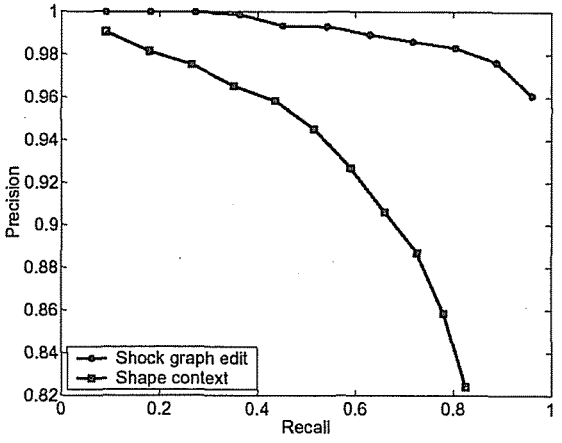

B. Large Databases (Sebastian etal. ECCV `02, ICPR `02)

- **1032 shapes**, 0.5 million matches (**Recognition rate: 99%)**
- => categorization/clustering
- **Metric space**: Embedded only as a high dimensional Euclidean space. Therefore spatial access method not efficient
- Showed **coarse-to-fine** matching. **Recognition rate: 90% or better but not 100%.**
- 26000 shape database constructed.

C. Skeleton vs. Curves and other representations (Sebastian et al PAMI `01)

- Introduced the notion of "**alignment curve**" for symmetric treatment of curves
- Very good **matches, morphing, average curves**
- But difficulty in rearranged parts, misses regional interactions

**1032 Shape Database**

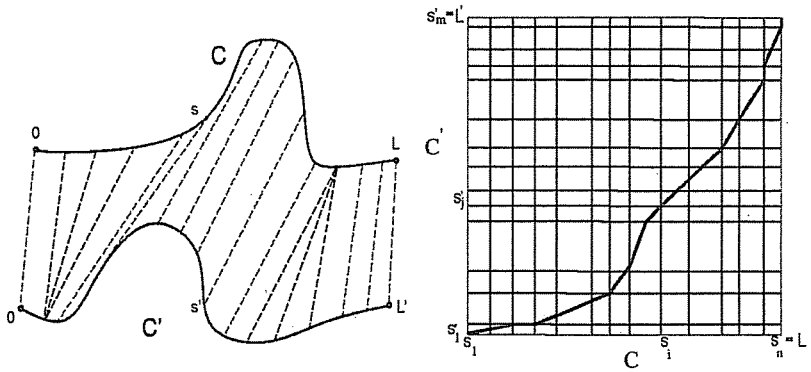


**The "Alignment Curve"**

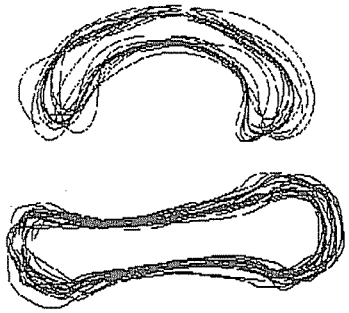

**Curve Averaging**

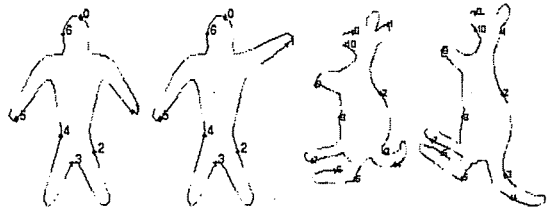

**Shape Matching using curves**

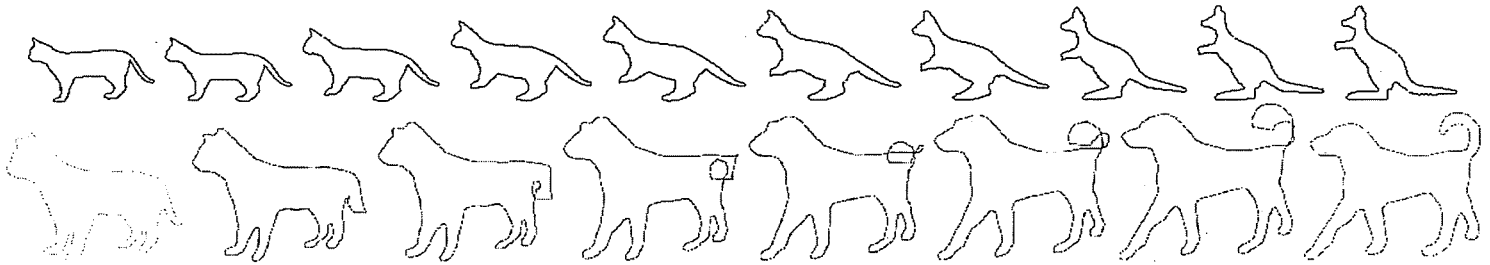

**Shape Morphing using the "Alignment Curve"**

D. Complete Language for shape

- **Intrinsic reconstruction** of shape from differential geometry of shocks (Giblin, Kimia PAMI `01)
- Need for global reconstruction.

E. 3D Recognition: Similarity based Aspect Graphs (IJCV `01)

- A basin of similarity allows for a clustering of view into aspects, but using grouping not transitions.
- Not restricted to general shapes
- Not affected by small scale structure

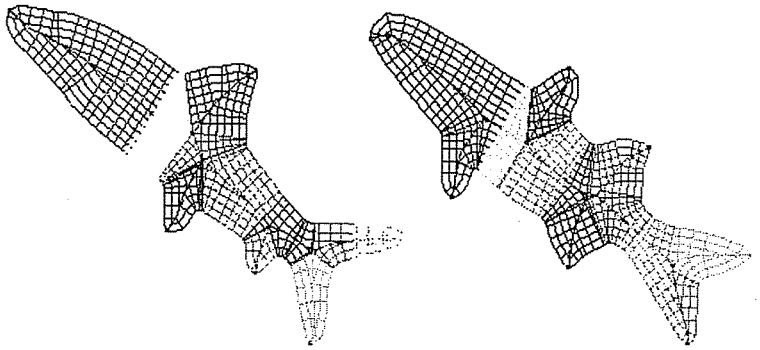

**Intrinsic Shape Coordinate System**

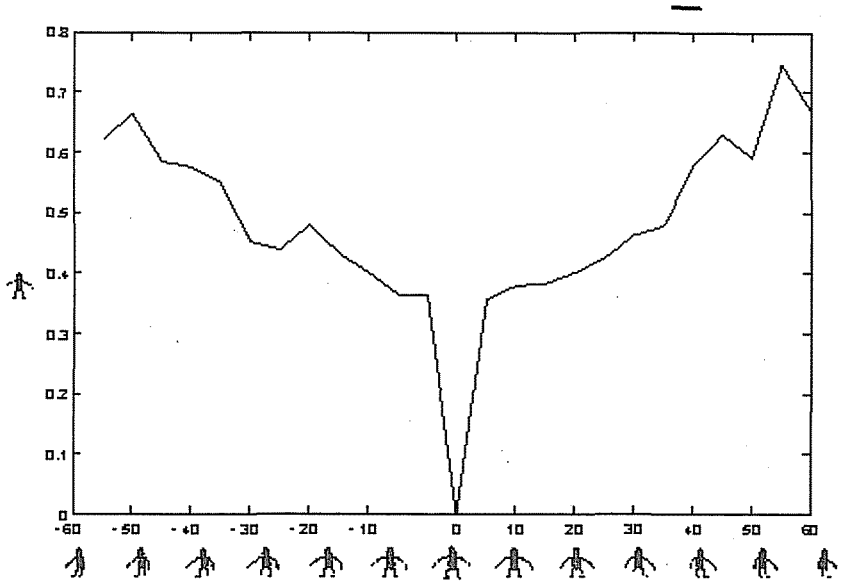


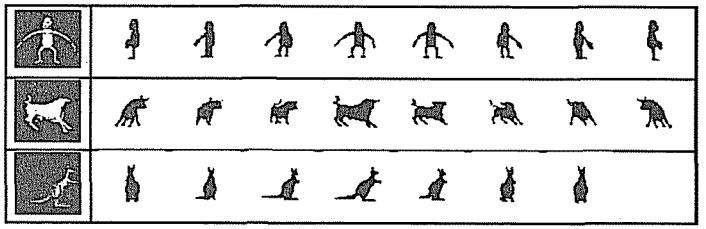

**3D shape and its aspect views**

| Unknown | Match 1 | Match 2 | Match 3 | Match 4 | Match 5 |
|---|---|---|---|---|---|
| | 0.269 | 0.497 | 0.512 | 0.526 | 0.567 |
| | 0.536 | 0.703 | 0.708 | 0.726 | 0.744 |
| | 0.376 | 0.623 | 0.625 | 0.637 | 0.640 |

## 2. Segmentation and Perceptual Grouping

A. Skeletally Mediated Deformable Models (**SCDM**) (MIA `03)

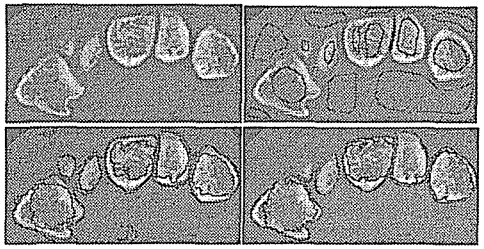

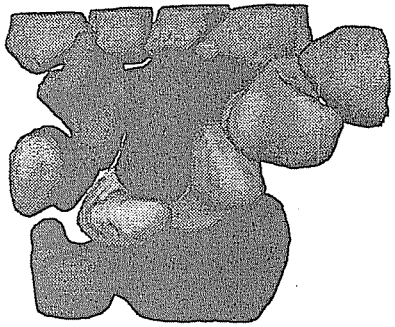

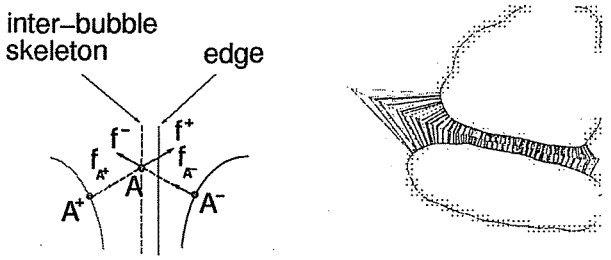




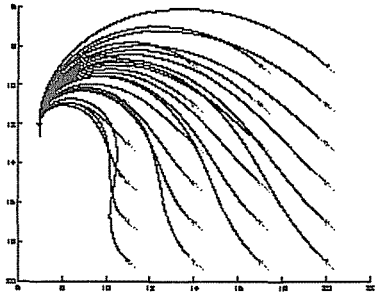

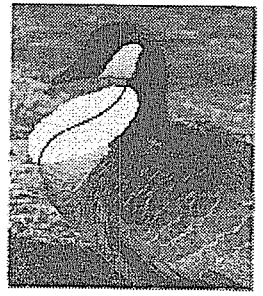

B. **Euler Spiral interpolation** of edge elements (IJCV `01)

C. **Corner preserving smoothing** via shock transforms (JMIV `01)

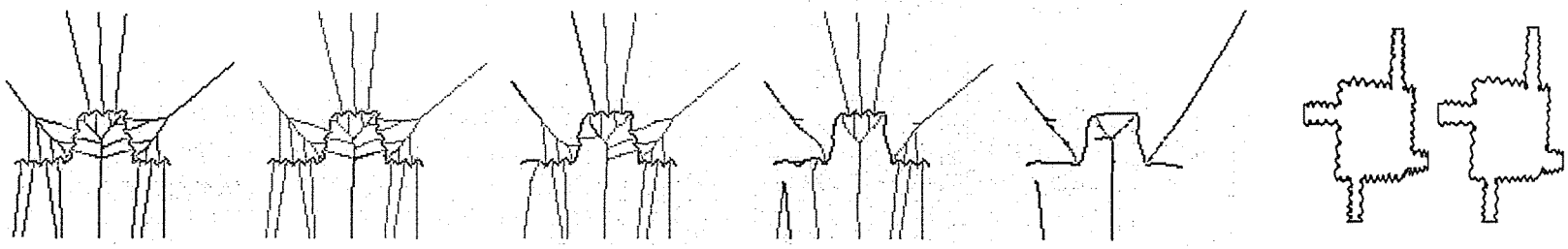

D. **Perceptual Grouping** via shock transforms (POCV `01)

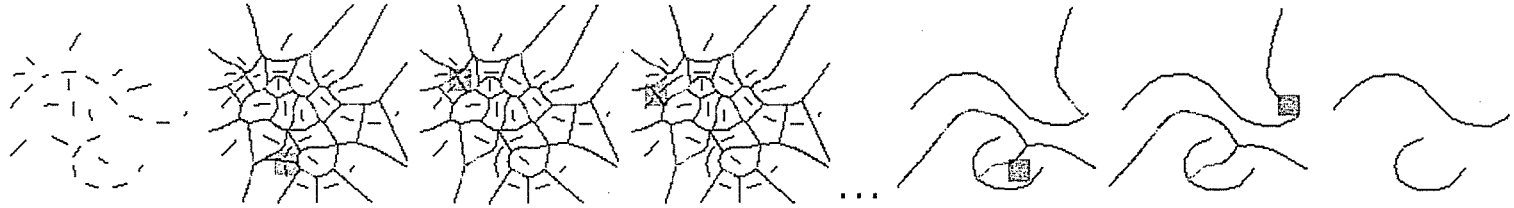

# 3. 3D Shape Representation via shock scaffold

- Need for summarizing MA complex of connected sheets as a graph

A. Formal classification of **Local Form** of 3D shocks (Giblin: Kimia PAMI '04)

B. Shock Scaffold: Network of Points and curves (IWVF `01)

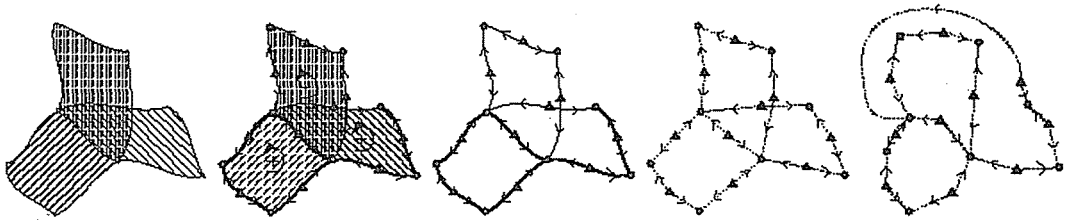

(a) $\mathcal{MA}$ (b) $\mathcal{SC}^+$ (c) $\mathcal{SC}$ (d) $\mathcal{SC}^-$ (e) $\mathcal{TS}$

C. Computation of **shock scaffold** for unorganized point cloud (CVPR '03)

D. Formal classfication of **transitions** of 3D shocks (Giblin Kimia ECCV '02)

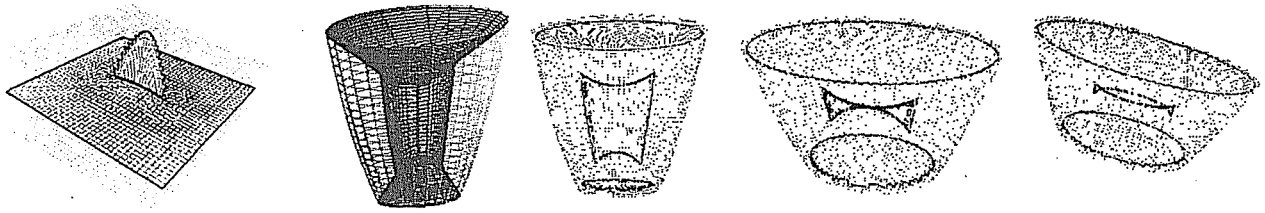

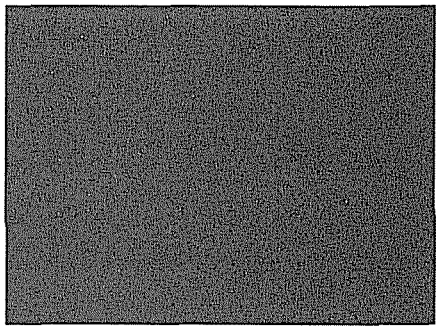

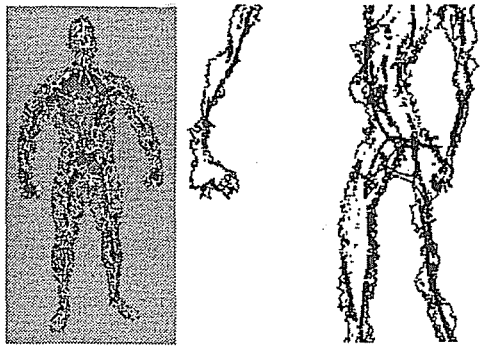

| Transition | Collision of Types |
|---|---|
| $A_1^4$ | $A_1^3$ - $A_1^3$ |
| $A_1^5$ | $A_1^4$ - $A_1^4$, $A_1^4$ - $A_1^3$ |
| $A_5$ | $A_1A_3$ - $A_1A_3$, $A_3$ - $A_3$ |
| $A_1A_3 - I$ | $A_1A_3$ - $A_1A_3$ |
| $A_1A_3 - II$ | $A_1A_3$ - $A_1A_3$, $A_1^3$ - $A_3$ |
| $A_1^2A_3 - I$ | $A_1^4$ - $A_1A_3$ |
| $A_1^2A_3 - II$ | $A_1^3$ - $A_1A_3$ |

# Brief Review of Kimia's Research Activities at LEMS

- Medical Imaging
- Archeology: Fragment Assembly
- Exploring Visual Perception and Modeling Cortical Activity
- Video Surveillance
- Shape Representation and Recognition

# Object Recognition: role of medial axis

Overview:

- Shock Graph Representation of Shape
- Reconstruction of Shapes from Shocks
- Transitions of the Medial Axis (*MA*) / Shock Graph (*SH*)
- Recognition as the Least Action Deformation Path: equivalent classes based on transitions
- Search via Graph Edit Distance
- Recognition results:
  - Robustness under visual transformations
  - Indexing into shape databases
- 3D Shock Scaffold and Transitions

# Symmetry-based Representation of Shape

- Blum's Medial Axis (*MA*):
  - Quench points of a grassfire initiated at boundary
  - Locus of centers of maximal inscribed circles
  - Geometry of axis plus radial information provides complete information about shape
- Symmetry Set (*SS*): locus of centers of circles with at least two distinct points of contact [Bruce and Giblin 1985]
- Other Symmetry Representations: cordal axis, PIZA, etc.
- Shock Graph (*SH*):
  - View the locus as singularities of flow (shocks)
  - Augments the classification to include this
  - Examples of shock graphs

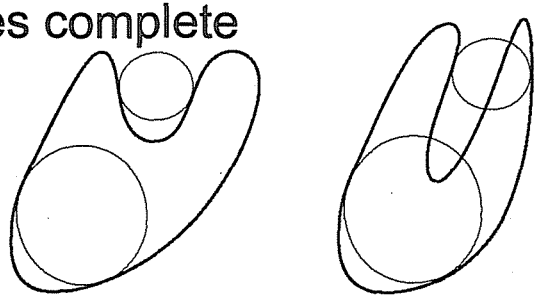

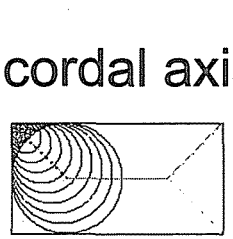

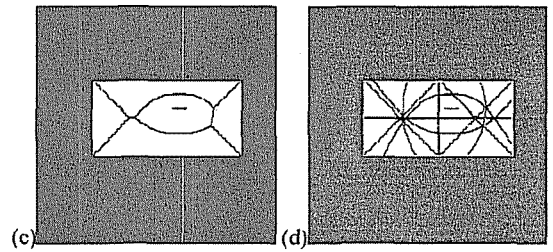


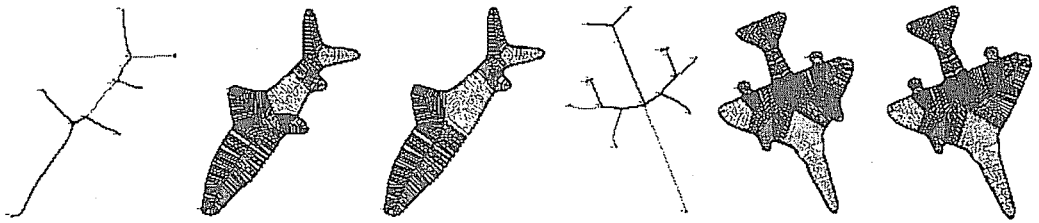

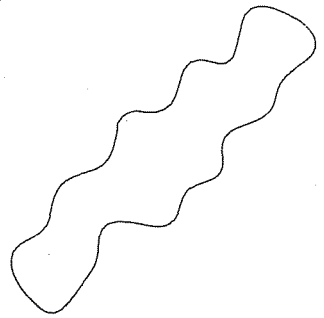

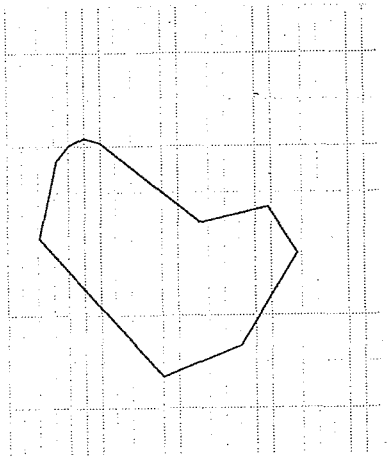

# Dynamic Visibility in a PDE based Implicit Framework

TSAI, Y. H. Richard

**Abstract**

I will present a PDE based, multi-level, algorithm for computing the visibility (the view *frustrum*) *on* the grid. Under this framework, I will discuss how the occlusion boundaries move according to the motion of the vantage point. Finally, I will propose a variational strategy for the type of problems, such as surveillance, involving complete visibility with or without memory, and poissibly with multiple vantage points.

# Linear and Nonlinear Subpixel Superresolution Techniques

Akihiko Torii† and Atsushi Imiya††

†School of Science and Technology, Chiba University, Japan
††National Institute of Informatics, Japan
Institute of Media and Information Technology, Chiba University, Japan

## Abstract

*In this paper, we introduce two methods for superresolution of discrete images. One is a linear method based on the inverse of the pyramid transform, and the other is a nonlinear method based on partial differential equation.*

## 1. Introduction

In this paper, we introduce two methods for superresolution of discrete images. One is a linear method based on the inverse of the pyramid transform, and the other is a nonlinear method based on partial differential equations.

The low-resolution property of observed data is a fundamental limitation of the nano-scale vision problem. For the applications of established algorithms in computer vision and pattern recognition to the nano-scale imaging, it is required to design method for the construction of high-resolution images from low-resolution observations.

In the astronomy [1] and classical medical imaging, for the construction of accurate and reliable images, many superresolution techniques and enhancement method were proposed. Well-established computational superresolution techniques are based on the extrapolation in the frequency domain [2, 3, 4], because most of the observation systems in astronomy and medical imaging are modeled and act as the low pass filters [2]. Gerchberg [3] and Youla [4] introduced an extrapolation method based on the successive projections to subspaces which are defined from constraints of data and imaging systems. The same method was also applied to the image reconstruction from the limited view angle data in tomographic imaging [5].

A well established linear enhancement method is based on the equation,

$$g = f - \alpha \Delta f, \tag{1}$$

where $\Delta$ and $\alpha$ are the Laplacian operator and a positive constant. This method enhances edges. Functions in the linear scale space are deformed as the solutions of the equation

$$f(\boldsymbol{x}, \tau) = e^{\alpha \Delta \tau} f(\boldsymbol{x}), \tag{2}$$

if we accept the Lie group framework for the linear-scale spaces [6]. Therefore, the formal inverse of the Gaussian-Kernel-base blurring is expressed as

$$e^{-\alpha \Delta \tau} = I - \alpha \Delta + \frac{(\alpha \Delta)^2}{2!} \cdots, \tag{3}$$

where $I$ is the identity operator. This expression implies that, the operator $I - \alpha\Delta$ is an approximation of the inverse of blurring by Gaussian-Kernel transform, which acts as a low-pass filter. The pyramid transform [7] is a discrete version of the blurring by Gaussian-Kernel transform. Therefore, the inverse of the pyramid transform acts as a superresolution procedure.

Since some interpolation methods derive smoothed images from samples [8], we need methods which construct sharp images controlling over-smoothing of images. The gray-values of image determines a terrain surface. Curvature flow is a method to enhance this terrain surface using local and global curvature information on the surface [9].

In this paper, we first introduce the inverse of the pyramid transform as a linear-superresolution technique. The technique derive a subpixel accurate images from a discrete image. The other one is PDE based method based on curvature flow of terrain. The method constructs high-resolution image by deforming surfaces of gray values of images.

## 2. Linear Superresolution

### 2.1. Pyramid Transform

Setting $x$-$y$ to be an orthogonal coordinate system on the Euclidean plane $\mathbf{R}^2$, we write a vector on $\mathbf{R}^2$ as $\boldsymbol{a} = (\alpha, \beta)^\top$, where $\boldsymbol{x}^\top$ is the transpose of vector $\boldsymbol{x}$. Points for which both coordinates are integers are called lattice points on $\mathbf{R}^2$ and the set of all lattice points is denoted by $\mathbf{Z}^2$. An image defined on $\mathbf{R}^2$ is

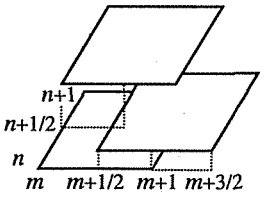


Figure 1: The relation of the two grid planes.

denoted by $f(x,y)$, where $f(x,y)$ is the gray-scale of an image at a point $\boldsymbol{x} = (x,y)^\top$.

Images which take constant values in small regions called pixels are called digital images. Our pixels are unit square domains $\mathbf{U}_{m\,n}$,

$$\mathbf{U}_{m\,n} = \{(x,y)^T | m-\frac{1}{2} \le x \le m+\frac{1}{2}, n-\frac{1}{2} \le y \le n+\frac{1}{2}\}, \tag{4}$$

of which centroids are lattice points.

Setting

$$u_{mn}(x,y) = \begin{cases} 1 & \text{if } \boldsymbol{x} \in int\,(\mathbf{U}_{m\,n}) \\ \frac{1}{2} & \text{if } \boldsymbol{x} \in \partial\mathbf{U}_{m\,n} \setminus \boldsymbol{v}_{m\,n} \\ \frac{1}{4} & \text{if } \boldsymbol{x} \in \mathbf{v}_{m\,n} \\ 0 & \text{if } \boldsymbol{x} \in \overline{\mathbf{U}_{m\,n}}, \end{cases} \tag{5}$$

where $\partial\mathbf{U}_{m\,n}$ is the boundary of $\mathbf{U}_{mn}$,

$$int\,(\mathbf{U}_{m\,n}) = \mathbf{U}_{m\,n} \setminus \partial\mathbf{U}_{m,n}, \tag{6}$$

and

$$\boldsymbol{v}_{m\,n} = \{(m+\varepsilon,\, n+\varepsilon)^\top \,|\, \varepsilon = \pm\frac{1}{2}\}, \tag{7}$$

the average of $f(x,y)$ in $\mathbf{U}_{mn}$ is obtained as

$$f(m,n) = \frac{1}{4}\int_{-\infty}^{\infty}\int_{-\infty}^{\infty} f(x,y)\, u_{mn}(x,y)dxdy. \tag{8}$$

In this equation, we can set $u_{mn}(x,y) = u_{0\,0}(x-m, y-n)$. Denoting $f(m,n)$ such that $(m,n)^\top \in \mathbf{Z}^2$ by $f_{mn}$, we call $f_{mn}$ the gray scale of pixel $(m,n)^\top$.

Setting

$$\overline{k}(m) = \frac{m}{2^{k-1}} \tag{9}$$

for $k \ge 1$ and $(m,n) \in \mathbf{Z}^2$, we define lattice points of the $k$-th order by

$$\boldsymbol{Z}^2{}_{(k)} = \{(\overline{k}(m),\, \overline{k}(n))^\top | (m,n)^\top \in \boldsymbol{Z}^2\}. \tag{10}$$

Therefore, $\mathbf{Z}^2_{(1)}$ is equivalent to $\mathbf{Z}^2$. Thus, we call $\mathbf{Z}^2_{(2)}$ the set of sublattice points. Figure 1 illustrates the relation between $\mathbf{Z}^2_{(1)}$ and $\mathbf{Z}^2_{(2)}$.

Let a pixel of the $k$-th order, of which the length of each edge is $1/2^{k-1}$, be

$$\mathbf{U}^{(k)}(a,\,b) = \{(x,y)^\top | a \le x \le a+\frac{1}{2^{k-1}}, b \le y \le b+\frac{1}{2^{k-1}}\}. \tag{11}$$

We call $\mathbf{U}^{(1)}(a,\,b)$ and $\mathbf{U}^{(2)}(a,\,b)$ a pixel and a subpixel, respectively. Vertexes of $\mathbf{U}^{(k)}(a,\,b)$ are located at $(a,b)^\top$, $(a+1/2^{k-1},b)^\top$, $(a+1/2^{k-1},b+1/2^{k-1})^\top$, and $(a,b+1/2^{k-1})^\top$. Then, we define the vertex set of a pixel of $k$-th order by

$$\boldsymbol{v}^{(k)}(a,\,b) = \{(a+\varepsilon, b+\varepsilon)^\top | \varepsilon = 0 \text{ or } \frac{1}{2^{k-1}}\}. \tag{12}$$

$\mathbf{U}^{(k)}(\overline{k}(m),\, \overline{k}(n))$ and $\mathbf{U}^{(k+1)}(\overline{k+1}(m),\, \overline{k+1}(n))$ satisfy the relations

$$\begin{aligned} &\mathbf{U}^{(k)}(\overline{k}(m),\, \overline{k}(n)) \\ &= \mathbf{U}^{(k+1)}(\overline{k+1}(2m),\, \overline{k+1}(2n)) \\ &\bigcup \mathbf{U}^{(k+1)}(\overline{k+1}(2m+1),\, \overline{k+1}(2n)) \\ &\bigcup \mathbf{U}^{(k+1)}(\overline{k+1}(2m+1),\, \overline{k+1}(2n+1)) \\ &\bigcup \mathbf{U}^{(k+1)}(\overline{k+1}(2m),\, \overline{k+1}(2n+1)) \end{aligned} \tag{13}$$

and

$$\begin{aligned} &\mathbf{U}^{(k+1)}(\overline{k+1}(2m+1),\, \overline{k+1}(2n+1)) \\ &\quad = \mathbf{U}^{(k)}(\overline{k}(m),\, \overline{k}(n)) \\ &\quad \bigcap \mathbf{U}^{(k)}(\overline{k}(m+1),\, \overline{k}(n)) \\ &\quad \bigcap \mathbf{U}^{(k)}(\overline{k}(m+1),\, \overline{k}(n+1)) \\ &\quad \bigcap \mathbf{U}^{(k)}(\overline{k}(m),\, \overline{k}(n+1)). \end{aligned} \tag{14}$$

Figure 1 illustrates the relation expressed by eqs. (13) and (14). Thus, a pixel of the $k$-th order can be expressed as a union of four pixels of the $(k+1)$-th order. Conversely, a pixel of the $(k+1)$-th order can be expressed as an intersection of four pixels of the $k$-th order.

Next, for $k \ge 1$ and $(a,b)^\top \in \mathbf{R}^2$, we define the function $u^{(k)}_{a\,b}(x,y)$ by

$$u^{(k)}_{a\,b}(x,y) = \begin{cases} 1 & \text{if } \boldsymbol{x} \in int\,(\mathbf{U}^{(k)}(a,\,b)) \\ \frac{1}{2} & \text{if } \boldsymbol{x} \in \partial\mathbf{U}^{(k)}(a,\,b) \setminus \mathbf{v}^{(k)}(a,\,b) \\ \frac{1}{4} & \text{if } \boldsymbol{x} \in \mathbf{v}^{(k)}(a,\,b) \\ 0 & \text{if } \boldsymbol{x} \in \overline{\mathbf{U}^{(k)}}(a,\,b), \end{cases} \tag{15}$$

where

$$int\left(\mathbf{U}^{(k)}(a,\,b)\right) = \mathbf{U}^{(k)}(a,\,b) \setminus \partial\mathbf{U}^{(k)}(a,\,b) \tag{16}$$

and $\partial \mathbf{U}^{(k)}(a, b)$ is the boundary of $\mathbf{U}^{(k)}(a, b)$. We call $u^{(k)}_{\overline{k}(m)\,\overline{k}(n)}(x, y)$ the base functions of the $k$-th order. A digital image of the $k$-th order is defined by

$$f^{(k)}(x, y) = \sum_{(m,n)^\top \in \boldsymbol{Z}^2} f^{(k)}_{\overline{k}(m)\,\overline{k}(n)}\, u^{(k)}_{\overline{k}(m)\,\overline{k}(n)}(x, y), \quad (17)$$

where each gray-level $f^{(k)}_{k(m),k(n)}$ is a real value. Furthermore, we call $f^{(1)}(x, y)$ and $f^{(2)}(x, y)$ a digital image and a sub-digital image, respectively. In the following, we will be concerned with digital images which are always zero outside of regions

$$\boldsymbol{D}^{(k)} = \bigcup_{(\overline{k}(m),\overline{k}(n))^\top \in \boldsymbol{S}^{(k)}} \mathbf{U}^{(k)}(\overline{k}(m), \overline{k}(n)). \quad (18)$$

Here, set $\boldsymbol{S}^{(k)}$ is an appropriate finite subset of ROI $\boldsymbol{S}$ for each $k \geq 1$.

Equation (13) leads to a relation between functions $u^{(k)}_{\overline{k}(m)\,\overline{k}(n)}(x, y)$ and $u^{(k+1)}_{\overline{k+1}(m')\,\overline{k+1}(n')}(x, y)$,

$$\begin{aligned} u^{(k)}_{\overline{k}(m)\,\overline{k}(n)}(x, y) &= u^{(k+1)}_{\overline{k+1}(2m)\,\overline{k+1}(2n)}(x, y) \\ &+ u^{(k+1)}_{\overline{k+1}(2m+1)\,\overline{k+1}(2n)}(x, y) \\ &+ u^{(k+1)}_{\overline{k+1}(2m+1)\,\overline{k+1}(2n+1)}(x, y) \\ &+ u^{(k+1)}_{\overline{k+1}(2m)\,\overline{k+1}(2n)}(x, y). \quad (19) \end{aligned}$$

Therefore, this equation shows that a base function of the $k$-th order is a linear sum of four base functions of the $(k + 1)$-th order. Therefore, if the condition

$$\begin{aligned} f^{(k+1)}_{\overline{k+1}(2m)\,\overline{k+1}(2n)} &= f^{(k+1)}_{\overline{k+1}(2m+1)\,\overline{k+1}(2n)} \\ &= f^{(k+1)}_{\overline{k+1}(2m+1)\,\overline{k+1}(2n+1)} \\ &= f^{(k+1)}_{\overline{k+1}(2m)\,\overline{k+1}(2n)}, \quad (20) \end{aligned}$$

is held, eq. (19) enables us to express a digital image of the $(k + 1)$-th order as a digital image of the $k$-th order. Conversely, eq. (19) also enables us to express a digital image of the $k$-th order as a digital image of the $(k + 1)$-th order.

## 2.2. Subpixel Superresolution

Let

$$\boldsymbol{L}^{(k)}_{0\,0} = \boldsymbol{Z}^2_{(k)}, \quad (21)$$

$$\boldsymbol{L}^{(k)}_{0\,1} = \{(a,\, b + \frac{1}{2^k})^T | (a, b)^T \in \boldsymbol{L}^{(k)}_{0\,0}\}, \quad (22)$$

$$\boldsymbol{L}^{(k)}_{1\,1} = \{(a + \frac{1}{2^k},\, b + \frac{1}{2^k})^T | (a, b)^T \in \boldsymbol{L}^{(k)}_{0\,0}\}, \quad (23)$$

and

$$\boldsymbol{L}^{(k)}_{1\,0} = \{(a + \frac{1}{2^k},\, b)^T | (a, b)^T \in \boldsymbol{L}^{(k)}_{0\,0}\}. \quad (24)$$

For $\{\alpha, \beta\} = \{0, 1\}, \{1, 1\}$, and $\{1, 0\}$, $\boldsymbol{L}^{(k)}_{\alpha\,\beta}$ is the translation of $\boldsymbol{L}^{(k)}_{0,0}$ by vector $(\alpha, \beta)^\top$. These sets of points define four types of pixel arrays. A pixel array which corresponds to $\boldsymbol{L}^{(k)}_{\alpha\,\beta}$ is obtained by translating the pixel array of which centroids are points in $\mathbf{Z}^2_{(k)}$ using vector $(\alpha, \beta)^\top$. Thus, pixels of which centroids are points in $\boldsymbol{L}^{(k)}_{\alpha\,\beta}$ and $\boldsymbol{L}^{(k)}_{\alpha'\,\beta'}$ overlap if the centroids are neighboring. Using these properties of pixels, we can derive a digital gray-scale image of which centroids of pixels are lattice points of $(k + 1)$-th order from four digital gray-scale images of which centroids of pixels are lattice points of $k$-th order. For proving these properties of digital images, it is sufficient to derive an algorithm which yields a subpixel digital image from four digital images.

Let $f(x, y)$ be a real-valued function defined in $\boldsymbol{R}^2$. The average of $f(x, y)$ in $\mathbf{U}^{(k)}(a, b)$ is obtained by

$$g^{(k)}_{\overline{k}(m)\,\overline{k}(n)} = \frac{1}{2^{2k}} \int_{-\infty}^{\infty} \int_{-\infty}^{\infty} f(x, y)\, u^{(k)}_{\overline{k}(m)\,\overline{k}(n)}(x, y) dx dy \quad (25)$$

Thus, letting

$$f^{(k)}_{\overline{k}(m)\,\overline{k}(n)} = 2^{2k} g^{(k)}_{\overline{k}(m)\,\overline{k}(n)}, \quad (26)$$

Eq. (19) leads to the systems of equations

$$\begin{aligned} f^{(k)}_{\overline{k}(m)\,\overline{k}(n)} &= f^{(k+1)}_{\overline{k+1}(2m)\,\overline{k+1}(2n)} \\ &+ f^{(k+1)}_{\overline{k+1}(2m+1)\,\overline{k+1}(2n)} \\ &+ f^{(k+1)}_{\overline{k+1}(2m+1)\,\overline{k+1}(2n+1)} \\ &+ f^{(k+1)}_{\overline{k+1}(2m)\,\overline{k+1}(2n+1)}, \quad (27) \end{aligned}$$

$$\begin{aligned} f^{(k)}_{\overline{k}(m+1/2)\,\overline{k}(n)} &= f^{(k+1)}_{\overline{k+1}(2m+1)\,\overline{k+1}(2n)} \\ &+ f^{(k+1)}_{\overline{k+1}(2m+2)\,\overline{k+1}(2n)} \\ &+ f^{(k+1)}_{\overline{k+1}(2m+2)\,\overline{k+1}(2n+1)} \\ &+ f^{(k+1)}_{\overline{k+1}(2m+1)\,\overline{k+1}(2n+1)}, \quad (28) \end{aligned}$$

$$\begin{aligned} f^{(k)}_{\overline{k}(m+1/2)\,\overline{k}(n+1/2)} &= f^{(k+1)}_{\overline{k+1}(2m+1)\,\overline{k+1}(2n+1)} \\ &+ f^{(k+1)}_{\overline{k+1}(2m+2)\,\overline{k+1}(2n+1)} \\ &+ f^{(k+1)}_{\overline{k+1}(2m+2)\,\overline{k+1}(2n+2)} \\ &+ f^{(k+1)}_{\overline{k+1}(2m+1)\,\overline{k+1}(2n+2)}, \quad (29) \end{aligned}$$

$$
\begin{aligned}
f^{(k)}_{\overline{k}(m)\,\overline{k}(n+1/2)} &= f^{(k+1)}_{\overline{k+1}(2m)\,\overline{k+1}(2n+1)} \\
&\quad + f^{(k+1)}_{\overline{k+1}(2m+1)\,\overline{k+1}(2n+1)} \\
&\quad + f^{(k+1)}_{\overline{k+1}(2m+1)\,\overline{k+1}(2n+2)} \\
&\quad + f^{(k+1)}_{\overline{k+1}(2m)\,\overline{k+1}(2n+2)}. \qquad (30)
\end{aligned}
$$

These systems of linear recursive formulae enable us to recover the averages of $f(x,y)$ in $\mathbf{U}^{(k)}(a,b)$ from those in $\mathbf{U}^{(k+1)}(a,b)$. From the viewpoint of practical application, we are only interested in the solution of systems of linear recursive formulae for $k=1$. Thus, we can obtain $f^{(2)}_{m/2\,n/2}$ by computing systems of linear recursive formulae iteratively for $(m,n)^\top \in Z^2$.b The second method is to solve the systems of linear recursive formulae at each subpixel and to define the closed form of the solution.

Supposing

$$
f^{(1)}_{a\,0} = f^{(1)}_{0\,b} = f^{(1)}_{a\,1/2} = f^{(1)}_{1/2\,b}, \qquad (31)
$$

we obtain the following theorem.

**Theorem 1** *Let $\alpha$ and $\beta$ be 0 or 1/2. Then, defining*

$$
g^{\alpha\beta}_{m\,n} = f^{(1)}_{m+1/2+\alpha\,n+1/2+\beta} - f^{(1)}_{m+\alpha\,n+1/2+\beta}, \qquad (32)
$$

$$
h^{\alpha\beta}_{m\,n} = f^{(1)}_{m+1/2+\alpha\,n+\beta} - f^{(1)}_{m+\alpha\,n+\beta}, \qquad (33)
$$

*the solution of the systems of linear recursive formulae Eqs. (27), (28), (29), and (30) is*

$$
f^{(2)}_{m+\alpha\,n+\beta} = \sum_{i=0}^{m}\sum_{j=0}^{n}(g^{\alpha\beta}_{i\,j} - h^{\alpha\beta}_{i\,j}). \qquad (34)
$$

Equation (31) is valid if we prepare workspaces around the ROI.

If an image is observed using a CCD array of which each aperture function is $u^{(1)}_{0\,0}$, we can obtain the digital image of the first order; that is, we obtain $f^{(1)}_{m\,n}$ for each $(m,n)^\top \in Z^2$ in the ROI. Therefore, theorem 4 indicates that four digital images recover a digital image with subpixel accuracy if we observe four mutually shifted images $f^{(1)}(x,y)$, $f^{(1)}(x+1/2,y)$, $f^{(1)}(x+1/2,y+1/2)$, and $f^{(1)}(x,y+1/2)$. Furthermore, for each $(m,n)^\top \in Z^2$, $f^{(1)}_{m+1/2\,n}$, $f^{(1)}_{m+1/2\,n+1/2}$, and $f^{(1)}_{m\,n+1/2}$ are obtained by arrays shifted by vectors $(1/2,0)^\top$, $(1/2,1/2)^\top$, and $(0,1/2)^\top$, respectively. Thus, from the viewpoint of implementation of an observation system these four images can be observed using four arrays which obtain $f^{(1)}(x,y)$, $f^{(1)}(x-1/2,y)$, $f^{(1)}(x-1/2,y-1/2)$, and $f^{(1)}(x,y-1/2)$, respectively.

# 3. Resolution Conversion

## 3.1. Boundary Extraction

We deal with two- and three-dimensional discrete space $\mathbf{Z}^2$ and $\mathbf{Z}^3$, respectively. Here after, we call $\mathbf{R}^2$ and $\mathbf{R}^3$ two- and three-dimentional space. Therefore $\mathbf{Z}^2$ and $\mathbf{Z}^3$ are two- and three-dimentional discrete space, respectively. For $(k,m,n)^\top \in \mathbf{Z}^3$, we set $\mathbf{Z}^2_1(k)$, $\mathbf{Z}^2_2(m)$, and $\mathbf{Z}^2_3(n)$ as two-dimensional planes $x=k$, $y=m$, and $z=n$, respectively. Plane $\mathbf{Z}_i(\alpha)$ is perpendicular to $\boldsymbol{e}_i$ for $i=1,2,3$, for $\boldsymbol{e}_1=(1,0,0)^\top$, $\boldsymbol{e}_2=(0,1,0)^\top$, and $\boldsymbol{e}=(0,0,1)^\top$. For points $(m,n)^\top$ and $(k,m,n)^\top$ in $\mathbf{Z}^2$ and $\mathbf{Z}^3$, respectively, $(m',n')^\top$ and $(k',m',n')^\top$ such that

$$
\begin{aligned}
(m'-m)^2+(n'-n)^2 &\le 1 \\
(k'-k)^2+(m'-m)^2+(n'-n)^2 &\le 1, \qquad (35)
\end{aligned}
$$

are 4-connected and 6-connected points on a plane and in a space, respectively. Furthermore, for points $(m,n)^\top$ and $(k,m,n)^\top$ in $\mathbf{Z}^2$ and $\mathbf{Z}^3$, respectively, $(m',n')^\top$ and $(k',m',n')^\top$ such that

$$
(m'-m)^2+(n'-n)^2 \le 2,\ (k'-k)^2+(m'-m)^2+(n'-n)^2 \le 3, \qquad (36)
$$

are 8-connected and 26-connected points on a plane and in a space, respectively. We express them as $\mathbf{N}_4(\boldsymbol{x})$, $\mathbf{N}_8(\boldsymbol{x})$, $\boldsymbol{N}_6(\boldsymbol{x})$, and $\mathbf{N}_{26}(\boldsymbol{x})$.

In $\mathbf{Z}_\alpha(\beta)$, we express 4-connected points as $\mathbf{N}^4_\alpha(\beta)$. For $\boldsymbol{x}=(k,m,n)^\top$, the neighborhood in a space and on planes satisfies the relation

$$
\mathbf{N}_6(\boldsymbol{x}) = \mathbf{N}^4_1(k) \bigcup \mathbf{N}^4_2(m) \bigcup \mathbf{N}^4_3(n). \qquad (37)
$$

Here after, we affix 0 and 1 to points in $\mathbf{Z}^2$ and $\mathbf{Z}^3$, and our object is the collection of pixels and voxels in two- and three-dimentional space whose centers are points in $\mathbf{Z}^2$ and $\mathbf{Z}^3$. We set $\boldsymbol{x}=(m,n)^\top$

$$
\boldsymbol{u}(\boldsymbol{x}) = \begin{cases} 1, & |m-\frac{1}{2}| \le 1, \\ & \text{and } |n-\frac{1}{2}| \le 1, \\ 0, & \text{otherwise}, \end{cases} \qquad (38)
$$

and, $\boldsymbol{x}=(k,m,n)^\top$

$$
\boldsymbol{v}(\boldsymbol{x}) = \begin{cases} 1, & \text{if } |k-\frac{1}{2}| \le 1,\ |m-\frac{1}{2}| \le 1, \text{ and } |n-\frac{1}{2}| \le 1, \\ 0, & \text{otherwise}, \end{cases} \qquad (39)
$$

respectively. $\boldsymbol{u}(\boldsymbol{x})$ and $\boldsymbol{v}(\boldsymbol{x})$ is a pixel and a voxel, respectively, whose center is at $\boldsymbol{x}=(m,n)^\top$ and $\boldsymbol{x}=(k,m,n)^\top$. Therefore setting $\boldsymbol{F}$ to be the set of 1-points, our object is expressed as in two- and three-dimentional space

$$
\boldsymbol{D} = \bigcup_{\boldsymbol{x}\in\boldsymbol{F}} \boldsymbol{u}(\boldsymbol{x}),\ \boldsymbol{D} = \bigcup_{\boldsymbol{x}\in\boldsymbol{F}} \boldsymbol{v}(\boldsymbol{x}), \qquad (40)
$$

We call the boundary of $\boldsymbol{D}$ the edge polygon and the surface polyhedron, for the collection of pixels and voxels, respectively. The edge polygon and surface polyhedron are extracted as

$$\Delta \boldsymbol{F} = \{(\boldsymbol{F} \oplus \mathbf{N}_8) \setminus \boldsymbol{F}\} \bigcup \{\boldsymbol{F} \setminus (\boldsymbol{F} \ominus \mathbf{N}_8)\}, \quad (41)$$

$$\Delta \boldsymbol{F} = \{(\boldsymbol{F} \oplus \mathbf{N}_{26}) \setminus \boldsymbol{F}\} \bigcup \{\boldsymbol{F} \setminus (\boldsymbol{F} \ominus \mathbf{N}_{26})\} \quad (42)$$

where $\oplus$ and $\ominus$ are the Minkowski addition and subtraction, respectively, of two sets in a vector space.
Next, we define edge polygon and surfel polyhedron in $\mathbf{Z}^2$ and $\mathbf{Z}^3$, respectively, for a set of points $\boldsymbol{F}$, denoting $\lambda \boldsymbol{F} = \{\lambda \boldsymbol{x} \,|\, \boldsymbol{x} \in \boldsymbol{F}, \lambda > 0\}$. The edge polygon is extracted as follows.

- Search for a pair of vertices $\boldsymbol{p}_1$ and $\boldsymbol{p}_2$ on $\boldsymbol{u}(\boldsymbol{x})$ for the boundary of $\Delta \boldsymbol{F}$.
- Follow points which satisfy the relations $|\boldsymbol{p}_{i+1} - \boldsymbol{p}_i| = |\boldsymbol{p}_i - \boldsymbol{p}_{i-1}|$, and $(\boldsymbol{p}_{i+1} - \boldsymbol{p}_i)^\top (\boldsymbol{p}_i - \boldsymbol{p}_{i-1})$ is 0 or 1, for $i \leq 2$.

The surfel polyhedron of three-dimentional discrete object is obtained applying the procedure slice by slice in axes directions $(1,0,0)^\top, (0,1,0)^\top, (0,0,1)^\top$. Since we deal with the 6-connected discrete objects, for a plane $\mathbf{P}_i(k)$ which is a perpendicular vector $\boldsymbol{e}_i$ for $i = 1,2,3$, and passes through point $k\boldsymbol{e}_i$, the vertices of object $\mathbf{O}$ lie on the cross sections of object $\mathbf{O}$ with respect to $\mathbf{P}_i(k)$, and the degree of vertices is three or four. Furthermore, adjacent vertices of a vertex exist in the 6-neighborhood of the vertex, since we deal with 6-connected discrete objects. The surface polyhedron is extracted by applying this algorithm slice-by-slice in each $\mathbf{P}_i(k)$. For a terrain such that $z = f(x,y)$, we assume that we are dealing with discrete objects which are infinite in the direction of $(0,0,-1)^\top$. Figure 2 shows the boundary edgels and surfels of objects on a plane and in a space.

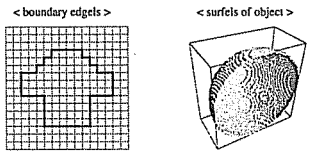


Figure 2: The edgel and the surfel of objects in 2D and 3D, respectively.

## 3.2. Generation of High-Resolution Images

We set an object $f(\boldsymbol{x})$, where $\boldsymbol{x} = (x,y)^\top$ and $\boldsymbol{x} = (x,y,z)^\top$ for two- and three-dimensional objects, respectively. We define the set of points $\boldsymbol{A} = \{\boldsymbol{x} \,|\, f(\boldsymbol{x}) > 1, \boldsymbol{x} \in \mathbf{R}^n\}$ in $\mathbf{R}^n$ for $n = 2,3$. Setting $f_m, \boldsymbol{m} \in \mathbf{Z}^n$ for $n = 2,3$ to be the average of volume of $f(\boldsymbol{x})$ in a pixel and a voxel in two- and three-dimentional space. The inverse quantization is to estimate $\boldsymbol{A}$ from $\boldsymbol{F} = \{\boldsymbol{m} \,|\, f_m > \frac{1}{2}\}$ and resolution conversion is described as the computation of $\frac{1}{m}\boldsymbol{F}_m$, where $\boldsymbol{F}_m$ is a binary set computed from the binary object $f(m\boldsymbol{x})$. Furthermore, set $\frac{1}{m}\boldsymbol{F}_m$ enables us to generate an approximation of high-resolution images of $f(\boldsymbol{x})$ for an arbitrary resolution. If $\boldsymbol{A}$ and its boundary $\partial \boldsymbol{A}$ is estimated from $\boldsymbol{F}$, it is easy to generate $\boldsymbol{F}_m$ by computing average in the pixels and the voxels where edge length is $\frac{1}{m}$ unit.

In the previous section, we proposed an algorithm for the estimation of boundary curve $\partial \boldsymbol{A}$ from digital set $\boldsymbol{F}$. Therefore, using the estimation $\overline{\boldsymbol{D}}$, we generate set $\frac{1}{m}\boldsymbol{F}_m$ according to the following steps.

1. Compute $\boldsymbol{D}$ from $\boldsymbol{F}$.
2. Compute the B-spline curve from $m\boldsymbol{D}$, and adopt its closure as the estimator of $m\partial \boldsymbol{A}$.
3. Apply the sampling scheme to the closure of the curve using unit pixels and voxels.
4. Reduce the size of pixels and voxels uniformly.

We propose algorithms for the estimation of $\overline{\boldsymbol{D}}$ in the next sections.

## 3.3. Deformation of Terrain

For vector $\boldsymbol{p}_{ij} = (i,j,f(i,j))^\top$, $i,j = 1,2,\cdots,n$, setting

$$D_1^2 \boldsymbol{p}_{ij} = \boldsymbol{p}_{i+1\,j} - 2\boldsymbol{p}_{ij} + \boldsymbol{p}_{i-1\,j},\ D_2^2 \boldsymbol{p}_{ij} = \boldsymbol{p}_{i\,j+1} - 2\boldsymbol{p}_{ij} + \boldsymbol{p}_{ij-1}, \quad (43)$$

we have the equation

$$D_1^2 \boldsymbol{p}_{ij} + D_2^2 \boldsymbol{p}_{ij} = (0,0,\Delta_4 f(i,j))^\top, \quad (44)$$

where $\Delta_4$ is the 4-connected discrete Laplacian operation for two-valued discrete function $f(i,j)$. Assuming that function $f(i,j)$ is a function of time $t$, we have the relation

$$\boldsymbol{p}_{ij}(t+1) - \boldsymbol{p}_{ij}(t) = (0,0,f(i,j,t+1) - f(i,j,t))^\top \quad (45)$$

Therefore, the equation

$$\boldsymbol{p}_{ij}(t+1) - \boldsymbol{p}_{ij}(t) = c(D_1^2 \boldsymbol{p}_{ij} + D_2^2 \boldsymbol{p}_{ij}), \quad (46)$$

where $c$ is a constant, implies the equation $f(i,j,t+1) - f(i,j,t) = \Delta_4 f(i,j,t)$. These mathematical properties of the deformation for discrete terrain data lead to the conclusion that our deformation for terrain data based

on the vertex Laplacian operation for a polyhedron is equivalent to the deformation by the linear diffusion equation, if we consider the height of each point as the gray-level of each point. Furthermore, equation (46) implies that, in the numerical computation, a serial application of the operations $D_1^2$ and $D_2^2$ is possible.

For the deformation of the discrete height model of a topographical map, we are required to preserve the height data of a map, since they depend on the measurement of heights. Therefore, we add new control points between data points of the discrete height model. Then, using these point as control points, we deform the model to derive a high-resolution level map.

Since a terrain is an open surface, its slices along the $x$ and $y$ axes are open curves in a space. Therefore, we consider the boundary conditions of Laplacian operator as open curves.

The new control points are generated according to the following rules.

1. For $i,j = 1,2,\cdots,n-1$, ${\boldsymbol{p}_{ij}}^{+} = (i+k, j+k, f(i,j))^{\top}$, where $0 < k < 1$.

2. For $i,j = 2,3,\cdots,n$, ${\boldsymbol{p}_{ij}}^{-} = (i-k, j-k, f(i,j))^{\top}$, where $0 < k < 1$.

3. For $i,j = 1,2,\cdots,n-1$, and if $|f(i+1,j) - f(i,j)| \geq 2k$, then ${\boldsymbol{p}_{ij}}^{\alpha} = (i+k, j+k, f(i,j)+\alpha l)^{\top}$, where $\alpha = 1,2,\cdots,\lceil l \rceil - 1$ and $l = \frac{|f(i+1,j)-f(i,j)|}{k}$.

4. For $i,j = 1,2,\cdots,n-1$, and if $|f(i,j+1) - f(i,j)| \geq 2k$, then ${\boldsymbol{p}_{ij}}^{\beta} = (i+k+\beta m, j+k\beta m, f(i,j)+\beta m)^{\top}$, where $\beta = 1,2,\cdots,\lceil m \rceil - 1$ and $m = \frac{|f(i,j+1)-f(i,j)|}{k}$.

We extract every point of intended resolution from the estimated discrete curves of each decomposed row and column and reconfigurate it as a form of the DTM matrix.

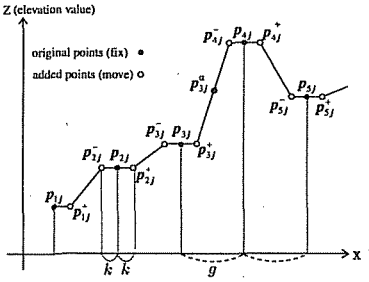


Figure 3: Control Point Generation.

# 4 Numerical Examples

Figure 4 shows the results of the resolution conversion of discrete terrain surface by our nonlinear method. In Figure 4, (a) shows the original topographical map which is a part of 1/5000 digital height map of a country. (b) shows a low-resolution map by reducing the original data points to 1/16. (c) shows a high-resolution map reconstructed from (b) by our super-resolution method. (d) shows a topographical map reconstructed from (b) by the traditional B-spline interpolation.

Since the positions and heights of local minima and maxima are cue-features for the evaluation of roughness of the interpolated functions, we computed the sum ratio $r_{\alpha\alpha}(i,j) = \frac{|\bar{f}_{\alpha\alpha}(i,j) - f_{\alpha\alpha}(i,j)|}{|f_{\alpha\alpha}(i,j)|} \times 100$ such that

$$r_{\alpha\alpha} = \sum_{(i,j)^{\top} \text{in the region of interest}} r_{\alpha\alpha}(i,j) \qquad (47)$$

for points $f_{\alpha\alpha}(i,j) = 0$, where $\alpha \in \{x,y\}$. Table 1 shows the sum of $r_{\alpha\alpha}(i,j)$ for all points in the region of interest.

In Figure 4, (e), (f), (g), and (h) are equi-level-contour representation of (a), (b), (c), and (d), respectively. The contour line is the collection of the same height-values of the terrain surface which is constructed from linear interpolation for discrete terrain surface. Equi-level-contour representation in Figure 4 illustrates the efficiency of our method which is the combination of deformation and interpolation.

We applied the superresolution to gray-value images considering the gray-values of images as the discrete terrain. Figure 5 shows the results of the superresolution of gray-value images. In Figure 5, (a), (b), (c), and (d) are the original image, the low-resolution image, the high resolution image reconstructed by our method, and the image reconstructed by B-spline interpolation for the low-resolution image, respectively. (e), (f), (g), and (h) are expanded parts of (a), (b), (c), and (d), respectively.

For the quantitative evaluation of the reconstructed image, we computed the average difference of gray values of images $r = \frac{1}{mn}\sum_{i=1,j=1}^{m,n} |f(i,j) - \bar{f}(i,j)|$, where $f(i,j)$ and $\bar{f}(i,j)$ are the gray values of the original and the reconstructed images, respectively. $mn$ is the size of the images. Table 1 shows the average difference $r$ for all points in the images.

Comparing (e) and (g) in Figure 5, our method for the superresolution efficiently works for the practical test images. In Figure 5, (e) and (g) show that our method recovers the small bright letters in the dark background and small parts in almost same gray values.

Table 1: The sum $r_{\alpha\alpha}$ of the ratio $r_{\alpha\alpha}(i,j)$ in figure 4 and the average difference $r$ of gray values in figure 5.

| | Figure 4 $r_{\alpha\alpha}$ | Figure 5 $r$ |
|---|---|---|
| (a) & (c) | 1.229 | 7.083 |
| (a) & (d) | 1.692 | 7.313 |

Figure 6 shows the results of the generation of uniform-resolution panoramic images employing the proposed nonlinear method for gray-level images. Figure 6 (a) shows SUEKAGE SOIOS 55-Cam which is the omnidirectional camera. This camera is constructed by the combination of a CCD sensor at 640 × 480 resolution and a hyperbolic-shaped mirror. Figure 6 (b) shows the omnidirectional image captured by the SOIOS. We extracted the useful range at 440 × 440. Figure 6 (c) is the result of the generation of uniform-resolution panoramic images using our curve estimation and resolution conversion. This panoramic image (c) has 1745 × 156 resolution. Furthermore, we generate a high-resolution image from this uniform-resolution panoramic image (c) in Figure 6 using the superresolution method for gray-level images. The resolution of the panoramic image is increased at 3490 × 312. Figure 6 (d) shows the magnified part of the superresolution panoramic image which has high and uniform resolution.

## 5. Conclusions

We have introduced two methods for superresolution of discrete images. One is a linear method based on the inverse of the pyramid transform, and the other is a nonlinear method based on partial differential equation. We have shown some results for superresolution for terrains and usual images. These results promiss that our method constructs high-resolution images from low-resolution observations for the applications of established algorithms in computer vision and pattern recognition to the nano-scale imaging.

The transformation of a panoramic image from an omnidirectional image requires the generation of the high- and uniform-resolution image from the low- and nonuniform-resolution omnidirectional image. It is possible for the generation of uniform- and high-resolution panoramic images to employ the superresolution method for gray-level images because our curve-estimation and resampling algorithms do not depend on the sampling rate. We showed the sufficient performance of our resolution-conversion method for the adaptation of omnidirectional images through numerical experiments.

## References


[1] Craig, I. J.D. and Brown, J. C., *Inverse Problems in Astronomy,* Adam Hilger; Bristol, 1986.

[2] Papoulis, A., A new algorithm in spectra analysis and band-limited extrapolation, IEEE, Trans, C&S, Vol. 22, 735-742, 1975.

[3] Gerchberg, R. W., Super-resolution through error energy reduction, Optica Acta, Vol. 22, 709-720, 1974.

[4] Youla, D. C., Generalized image restration by the method of orthogonal projections, IEEE, Trans, C&S, Vol. 25, 694-701, 1978.

[5] Lent, A., Tuy, H., An iterative method for the extrapolation of band-limited functions, J. Math. Anal. and Appl., Vol. 83, 554-565 1981.

[6] Sapiro, G., *Geometric Partial Differential Equations and Image Analysis,* Cambridge University Press, Cambridge, 2001.

[7] Jolion, J. M., Rosenfeld, A., *A Pyramid Framework for Early Vision,* Kluwer Academic Publishers; Dordrecht, 1994.

[8] Wahba, G., Surface fitting with scattered noisy data on Euclidean D-space and on the sphere, Rocky Mountain Journal of Mathematics, **14**, 281-299, 1984.

[9] Sethian, J. A., *Level Set Methods: Evolving Interfaces in Geometry Fluid Mechanics, Computer Vision, and Material Science.* Cambridge University Press, Cambridge, 1996.

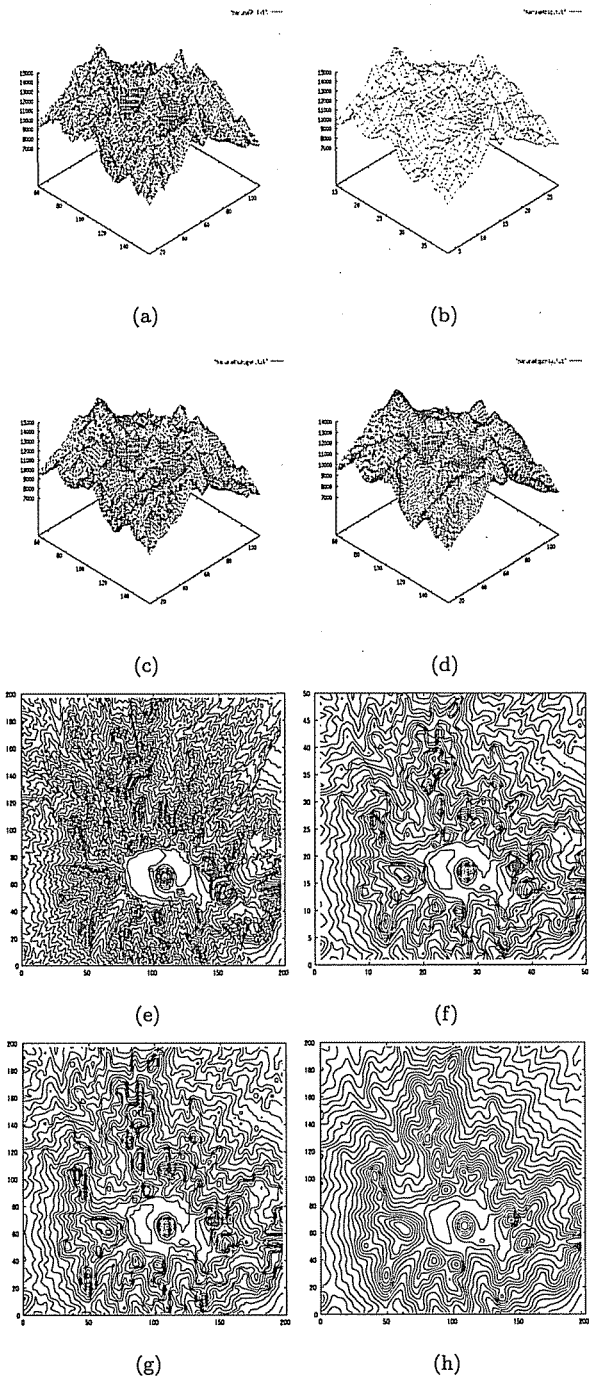


Figure 4: Superresolution for a Terrain: Digital Terrain Model raw data visualized by Gnuplot. (a) an original surface: 200 × 200 resolution. (b) the low resolution surface: 50 × 50 resolution. (c) the reconstructed surface by our superresolution method: 200 × 200 resolution. (d) the reconstructed surface without deformation process: 200 × 200 resolution. (e), (f), (g), and (h) are equi-level contour representation of (a), (b), (c), and (d), respectively.

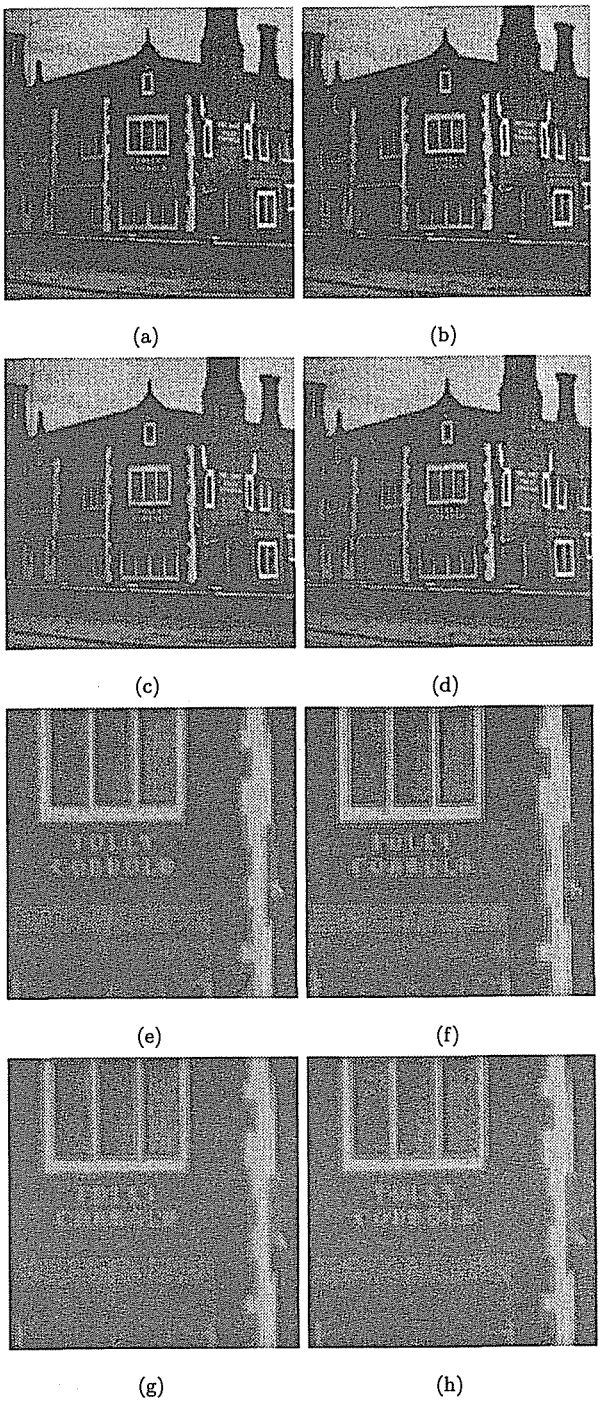


Figure 5: Superresolution for a 256 Gray-Value Image of House: (a) the original image: 512 × 512 resolution. (b) the low resolution image: 256 × 256 resolution. (c) the reconstructed image by our superresolution method: 512 × 512 resolution. (d) the reconstructed image without deformation process: 512 × 512 resolution. (e), (f), (g), and (h) are the expanded parts of (a), (b), (c), and (d), respectively.

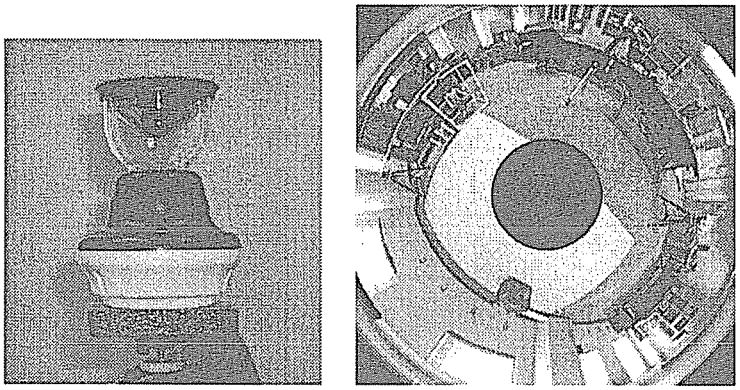

(a) (b)

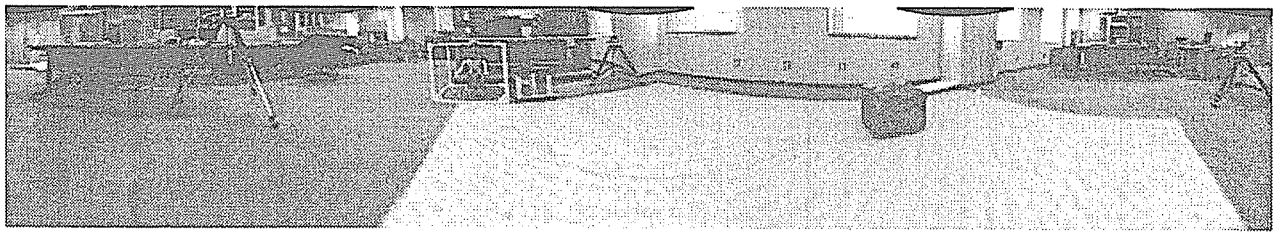

(c)

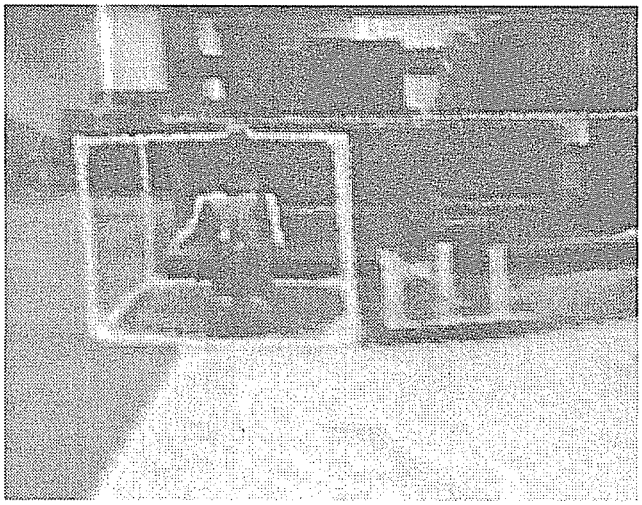

(d)

Figure 6: Generation of uniform-resolution panoramic images from omnidirectional images. (a) is SUEKAGE SOIOS 55-Cam. (b) is an omnidirectional image captured by SOIOS. The resolution is 440 × 440. (c) is the result of our generation of uniform-resolution panoramic images generated from (b) using the geometrical transformation and our resolution conversion. Since this panoramic image (c) still has low resolution, we generate a high-resolution image from this uniform-resolution panoramic image (c) using the superresolution method for gray-level images. The resolution of the high-resolution panoramic image is at 3490 × 312. (d) is the magnified part of the superresolution panoramic image. Comparing (b) and (d), our final result (d) preserves the connectivity and smoothness of edges of objects though the original resolution of (b) is low and nonuniform.

# GENERIC CENTRO-AFFINE DIFFERENTIAL GEOMETRY OF CURVES

TAKASHI SANO

Faculty of Engineering, Hokkai-Gakuen University

## 1. INTRODUCTION.

In [1] we have studied invariants for generic plane curves in Euclidean plane as an application of the singularity theory for Euclidean invariant functions.

Let $I \subset \mathbb{R}$ be an open interval and $\gamma : I \longrightarrow \mathbb{R}^2$ be unit speed. Then $\gamma'(s) = T(s)$ is a unit tangent vector of $\gamma$ and $N(s)$ is a unit normal vector to be obtained from $T(s)$ by rotating anticlockwise through $\frac{\pi}{2}$. There is a real number $\kappa(s)$ such that $T'(s) = \kappa(s)N(s)$, where $T'(s) = \frac{dT}{ds}(s)$. We call $\kappa(s)$ the curvature of $\gamma$ at $s$. Then we have the following theorem [1].

**Theorem 1.1.** *Let $\gamma : I \longrightarrow \mathbb{R}^2$ be a regular curve satisfying generic conditions (cf. [1]) and $p$ be a point of the evolute $\gamma(s) + \frac{1}{k(s)}N(s)$ of $\gamma$ at $s_0$. Then, locally at $p$, the evolute is*

(1) *diffeomorphic to a line in $\mathbb{R}^2$ if the point $\gamma(s_0)$ is not a vertex.*

(2) *diffeomorphic to an ordinary cusp in $\mathbb{R}^2$ if the point $\gamma(s_0)$ is an ordinary vertex.*

*where the ordinary vertex of a regular plane curve is corresponding to the stationary point of the curvature $\kappa(s)$.*

The ordinary cusp is a curve which is defined by $C = \{ (x_1, x_2) \in \mathbb{R}^2 \mid x_1^2 = x_2^3 \}$.

By arguments similar to those in Euclidean differential geometry, we have the theorem similar to Theorem 1.1.

Let $\mathbb{R}^2$ be an affine plane which adopt the coordinate such that the area of the parallelogram spanned by two vectors $a = (a_1, a_2)$, $b = (b_1, b_2)$ is given by $| \ a \ \ b \ | = a_1b_2 - a_2b_1$. There is a real number $\kappa_a(s)$ such that $\gamma'''(s) = -\kappa_a(s)\gamma'(s)$. We call $\kappa_a(s)$ the equi-affine curvature of $\gamma$ at $s$. Then we have the following theorem [3].

**Theorem 1.2.** *Let $\gamma : I \longrightarrow \mathbb{R}^2$ be a smooth plane curve satisfying $| \ \gamma'(s) \ \ \gamma''(s) \ | = 1$ and generic condition (cf. [3]) and $p$ be a point of the equi-affine evolute $\gamma(s) + \frac{1}{\kappa_a(s)}\gamma''(s)$ of $\gamma$ at $s_0$. Then, locally at $p$, the equi-affine evolute is*

(1) *diffeomorphic to a line in $\mathbb{R}^2$ if the point $\gamma(s_0)$ is not an equi-affine vertex.*

(2) *diffeomorphic to an ordinary cusp in $\mathbb{R}^2$ if the point $\gamma(s_0)$ is an ordinary equi-affine vertex.*

*where the ordinary equi-affine vertex of a plane curve is corresponding to the stationary point of the equi-affine curvature* $\kappa_a(s)$.

In this paper, we want to consider the theorem similar to Theorem 1.1 and Theorem 1.2 for the centro-affine structure.

All curves and maps considered here are of class $C^\infty$ unless otherwise stated.

## 2. Centro-affine differential geometry of plane curves

Let $\mathbb{R}^2$ be an affine plane. We define punctured 2-space to be the set of nonzero row vectors in $\mathbb{R}^2$ and we denote it by $\mathbb{R}^2_0$.

Let $\gamma : I \longrightarrow \mathbb{R}^2_0$ be a smooth regular curve with $\frac{|\ \ddot{\gamma}(t)\ \ \dot{\gamma}(t)\ |}{|\ \gamma(t)\ \ \dot{\gamma}(t)\ |} \neq 0$, where $\dot{\gamma}(t) = \frac{d\gamma}{dt}(t)$. If we reparametrize a given curve $\gamma$ by using $s(t) = \int_{t_0}^{t} \left( \frac{|\ \ddot{\gamma}(t)\ \ \dot{\gamma}(t)\ |}{|\ \gamma(t)\ \ \dot{\gamma}(t)\ |} \right)^{\frac{1}{2}} dt$, then the curve $\gamma$ satisfies that $\frac{|\ \gamma''(s)\ \ \gamma'(s)\ |}{|\ \gamma(s)\ \ \gamma'(s)\ |} = 1$.

By arguments similar to those in euqi-affine differential geometry, we have the following formula; $\gamma'''(s) = \kappa_1(s)\gamma'(s) \pm \kappa_2(s)\gamma''(s)$ where $\kappa_1(s) = \frac{|\ \gamma''(s)\ \ \gamma'''(s)\ |}{|\ \gamma''(s)\ \ \gamma'(s)\ |}$, $\kappa_2(s) = \frac{|\ \gamma'(s)\ \ \gamma'''(s)\ |}{|\ \gamma''(s)\ \ \gamma'(s)\ |}$. Then we have the following [5].

**Theorem 2.1.** *Let* $\gamma : I \longrightarrow \mathbb{R}^2_0$ *be a smooth plane curve satisfying* $\frac{|\ \gamma''(s)\ \ \gamma'(s)\ |}{|\ \gamma(s)\ \ \gamma'(s)\ |} = 1$ *and generic condition (cf.* [5]*) and* $p$ *be a point of the centro-affine evolute* $\gamma(s) + \frac{1}{\kappa_1(s)}\gamma''(s)$ *of* $\gamma$ *at* $s_0$. *Then, locally at* $p$, *the centro-affine evolute is*

(1) *diffeomorphic to a line in* $\mathbb{R}^2$ *if* $\kappa_1(s_0) \neq 0$ *and* $\sigma(s_0) \neq 0$.

(2) *diffeomorphic to an ordinary cusp in* $\mathbb{R}^2$ *if* $\kappa_1(s_0) \neq 0$, $\sigma(s_0) = 0$ *and* $\sigma'(s_0) \neq 0$.

*where* $\sigma(s) = \kappa_1'(s) - \kappa_1(s)\kappa_2(s)$.

## 3. Miscellanea

In this section, we consider the recognition problem. Then the contour is strong way, as the method of recognition of the object. Now, for the simply, we consider the convex curve as the contour. It is effective to use the "codons" for representations of the contour. So we introduce the codons. There are several articles which study about the codons in the Euclidean plane ([2, 4, etc.]).

All curve segments contain zero, one or two inflexion (the inflexion is the point satisfying $\kappa(s) = 0$ and $\kappa'(s) \neq 0$). Segments with no inflexions are called type 0 codons, those with two inflexions are called type 2 codons. If a segment has exactly one inflexion, the zero point of $\kappa(s)$ (with $\kappa'(s) \neq 0$) may be encountered either before or after the maximal point of the segment when traversing the curve in the chosen orientation. We call type $1^-$ codons if before and type $1^+$ codons if after. When we divide to four primitive codons, each segments $\gamma_i$ $(i = 1, 2, \cdots, n)$ are corresponding to the number $c_i \in \{0, 1^-, 1^+, 2\}$. Then we have the string of numbers $c_1c_2c_3\cdots c_n$ called the codon string.

However 2 convex curves have same codon string, these are not same curves (contour). Because the codons are defined by $\kappa(s)$. So it is difficult to restore the original curve by codon string only.

But there are several curvatures, that is, we have not only $\kappa(s)$ but also $\kappa_a(s)$, $\kappa_1(s)$, $\kappa_2(s)$ and so on. If we make new codons by $\kappa_a(s)$, $\kappa_1(s)$, $\kappa_2(s)$ and so on, we can restore the original curve by codon string and new codon string, probably. So author consider that we need to make new codons.

## References


1. J. W. Bruce and P. J. Giblin, *Curves and singularities*, Cambridge University press, 1984.
2. D. D. Hoffman and W. A. Richards, *Representing smooth plane curves for recognition : implications for figure-ground reversal*, Proc. Nat. Conf. on Art. Intell. AAAI **24** (1982), 5–8.
3. S. Izumiya and T. Sano, *Generic affine differential geometry of plane curves*, Proc. Edinburgh Math. Soc. **41** (1998), 315–324.
4. W. A. Richards and D. D. Hoffman, *Codon Constraints on Closed 2D shapes*, Computer vision, Graphics, and Image Processing **31** (1985), 265–281.
5. T. Sano, *Generic centro-affine differential geometry of plane curves*, preprint.



*E-mail address*: t-sano@cvl.hokkai-s-u.ac.jp *or* t-sano@math.sci.hokudai.ac.jp

# A Theory of Negative Shape : Revisited

DEGUCHI, Kohichiro (Tohoku University)
(joint work with P. Ghosh, NCST, India)
kodeg@fractal.is.tohoku.ac.jp

## Abstract

## 1 Introduction

Is it possible to do addition & subtraction (or multiplication & division) with geometric shapes as we do in ordinary arithmetic with numbers?

We observe that the resemblance between the integer number system with multiplication & division and the system of convex objects with Minkowski addition & decomposition is really striking. Now, to view multiplication and division as a single operation it became necessary to extend the integer number system to the rational number system. Exactly in the similar way, in order to unify the two Minkowski operations as a single operation, it is necessary that the ordinary convex object domain must be appended by a notion of inverse shape of objects or *negative shapes.* More interestingly, the concept of negative shapes permits further unification. A nonconvex object may be viewed as a *mixture* of ordinary convex shape object and negative shape object.

The first part of this presetation deals with the introduction of the notion of *negative shapes.* For all such shape manipulations, we show that a geometric approach to the Minkowski operations, called the *slope diagrammatic approach,* is particularly appropriate, instead of the conventional set theoretic approach.

Then, we present an idea of the shape decomposition into *prime shapes,* which are analogue of the prime numbers and indecomposable ones. Here, we concentrate the discussion on binary images, and present some propositions on the indecomposability problem.

## 2 Indecomposability problem

The problem we are given here is:

> Given a set of points $S$ in the plane, determine whether it can be expressed as a Minkowski sum of two simpler sets of points. In other words, are there sets of points $A$ and $B$ in the plane, such that a given $S$ can be expressed as $S = A \oplus B$ ?

Our motivation of this research is itemized as:

- An *indecomposable* shape is like a *prime number.* It can- not be decomposed further as a Minkowski sum of two simpler shapes.

- Exactly like the prime numbers, the indecomposable shapes may be considered as the fundamental building blocks of all geometric shapes. If one can identify the set of all indecomposable shapes $\{I_1, I_2, \ldots\}$, then any point set $S$ can be represented as a Minkowski sum of indecomposable shapes,

$$S = I_i \oplus \cdots \oplus I_k \tag{1}$$

- The basic hurdle, however, is to identify an indecomposable shape.

It should be noted that the indecomposability problem is concerned with the shape of an object. Here, we assume that all the translates of a gxven point set are equivalent. There are some trivial decompositions. For example, any singleton point set $\{p\}$ behaves like number 1, since always $S = S_p \oplus \{p\}$ . Other than this, if $S$ is a compact convex set in $E^d$ and if $\lambda$ denotes any real number greater than zero but less than one, then $\lambda S$ is a trivial summand of $S$, for $S = \lambda S \oplus (1 - \lambda)S$ . Such trivial decompositions are not considered as proper decompositions.

Earlier works for this problems are found as:

Indecomposability problem in the domain of convex poly- topes in $E^d$ has been studied by mathematicians. It has long been known that in the domain of convex polygons triangles (and line segments which are nothing but degenerate triangles) are the only indecomposable sets. For general convex polytopes in $E^d$ where $d > 3$, there do not exist any such simple, closed universal approximating classes.

Characterization of indecomposable polytopes in higher dimensions is a hard problem. Shephard found a sufficient (but not necessary) condition for a polytope to be indecomposable. Meyer later gave the necessary and sufficient condition for indecomposability of polytopes. Meyer's condition is expressed in terms of the rank of a certain set of linear homogeneous equations that can be formed from the supporting functions of a polytope. A simpler approach, yielding the same results, was presented by McMullen, using a translation-invariant representation of polytopes. Smilansky also proved similar results by introducing the concept of a dual of a polytope.

These approaches, except Shephard's, are highly *algebraic*, and it is difficult to get the geometric intuition of indecomposability from such treatments. Very little has so far been done in the discrete domain, even in the " lest domain of binary images. One may mention Kanungo and Haralick and Xu. We could not find any literature on indecomposability of nonconves objects – neither in any continuous nor in any discrete domain.

## 3 Our approach : weakly taxi-cab convex (WTC) polygons

To the problem above, our approach here is as follows.

We transform a binary image into a continuous polygon. For continuous polygon - convex or nonconvex - the *slope daiagram* technique is employed for computating Minkowski addition. Then, a convenient subset of all binary images is identified. It is termed the *weakly tasicab convex* (WTC) class of images. Computation of Minkowski addition of WTC images is then taken up. The computation technique immediately indicates a number of results concerning indecomposability of WTC polygons.

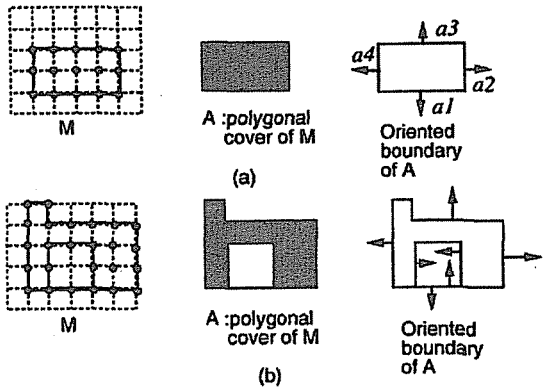


Binary images, their 4-connected polygonal covers, and the oriented boundaries of the covers.

We transform a binary image into a polygon by taking the 4-connecteri polygonal cover of the tmage. The 4-connected polygonal cover may be conceived in various other ways. One interesting way is to conceive it as, $Polygonal\_Cover(M) = (M \oplus Q) \ominus Q$ where $Q$ denotes a unit square regxon. We assume that the 4-connected polygonal cover $A$ is a complete representation of a binary image $M$. The length of every edge of a polygonal cover may be considered to be an integer number.

The reason for the need for a "nearly convex" domain is as followings: In the question of indecomposability, it is preferable to work with images which are "nearly convex". The rationale of this conviction comes from the following fact.

**Proposition 1** *Let $S$ be a convex set for which there do not exist convex sets $A$ and, $B$ such that $S = A \oplus B$. Then there cannot exist general sets $P$ and $Q$ such that $S = P \oplus Q$.*

If we work within the convex shape domain and discover that some shape $S$ is indecomposable within that domain, then $S$ is *intrinsically* indecomposable. Within the domain of 4-connected polygonal covers of binary images, the convex subdomain is not challenging.

**Definition 1 (Weakly taxicab convex polygon)** A 4-connected polygonal cover $A$ is called weakly taxicab conves (WTC) polygon if at least one taxicab line segment joining each pair of points of $A$ lies entirely in $A$.

A 4-connected polygonal cover which is monotone with respect to both the $x$-axis and the $y$-axis, is a weakly taxicab convex polygon.

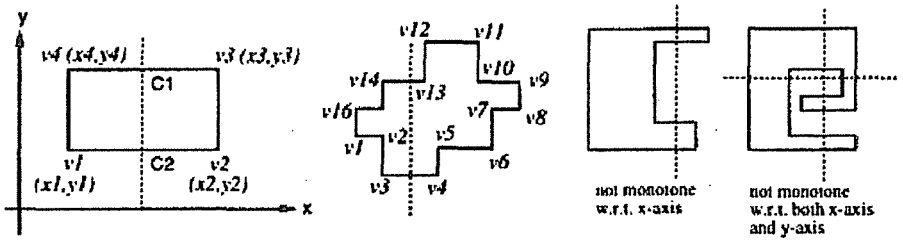


(a) Weakly taxicab convex polygonal covers (each polygon is monotone w.r.t. both x-axis and y-axis)

(b) Polygonal covers which are not weakly taxicab convex

# 4 Indecomposability results on the WTC polygons

## 4.1 A few properties of WTC polygons

Before presenting some results on the indecomposability results on the WTC polygons, we list a few properties of WTC polygons related to the Minkowski operations.

**Proposition 2** *If $A$ and, $B$ are two WTC polygons, their Minkowski sum $A \oplus B$ is also a WTC polygon.*

**Proposition 3** *If $A$ and $B$ are two WTC polygons, then their set intersection $A \cap B$ is either empty, or, one or more polygons each of which is a WTC polygon.*

**Proposition 4** *If $A$ is a WTC polygon then the Minkowski decomposition $A \ominus B$ is either empty, or, one or more WTC polygons.*

**Proposition 5** *If a WTC polygon $S$ is indecomposable in the WTC polygonal domain, it remains indecomposable even in the connected shape domain. (However, $S$ may be decomposable in the disconnected domain.)*

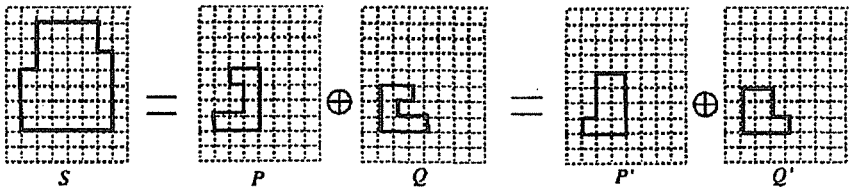


(a) Since S is decomposable in the connected domain, it is decomposable in the WTC domain too.

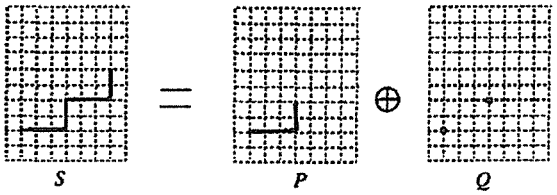


(b) S is indecomposable in the WTC domain, but decomposable in the general disconnected domain.

## 4.2 Representation of WTC polygons

For the WTC polygons the first advantage is that the boundary of every WTC polygon can be partitioned into eight angular regions, namely, O deg, between O deg and 90 deg, 90 deg, between 90 deg and 180 deg, 180 deg, between 180 deg and 270 deg, 270 deg, between 270 deg and 360 deg. We denote the four single direction angular regions by the symbols $i_1, i_2, i_3, i_4$, and the four 90 deg angular regions by the symbols $r_1, r_2, r_3, r_4$.

In any $i_j$-region the taxicab edge is referred to as an *$i_j$-edge*. An $i_j$-edge is completely specified by its length, say $\eta_j$. In $r_j$-region the taxicab edge of the polygon will consist of a monotonic chain of "steps". It is called an *$r_j$-edge* and its length is denoted by the symbol $x_j$.

If we assume that the angular regions will always be considered as a fixed ordered set $(i_1, r_1, i_2, r_2, \ldots, i_4, r_4)$, then the the WTC polygon can be completely expressed as an ordered 8-tuple:

$$\partial A = (\eta_1, x_1, \eta_2, x_2, \ldots, \eta_4, x_4).$$

This representation appears like a hypercomplex algebraic number.

## 4.3 A few results on indecomposability

41 Now, we show the results on indecomposability of WTC polygons.

**Proposition 6** *There are infinitely many indecomposable shapes.*

Our proof is analogous to Euclid's proof that there are infinitely many prtmes.

**Proposition 7** *Indecomposability or ciecomposability of a shape is invariant under every affine transformation.*

It implies that every rotated reflected or scaled image of an indecomposable shape is also indecomposable. For example, in the indecomposability question, WTC polygon $(\eta_1, x_1, \eta_2, x_2, \ldots, \eta_4, x_4)$ is equivalent to $(\eta_4, x_4, \eta_1, x_1, \ldots, \eta_3, x_3)$ which is obtained by circularly shifting the elements by two places. The shifting specifies a 90 deg rotation.

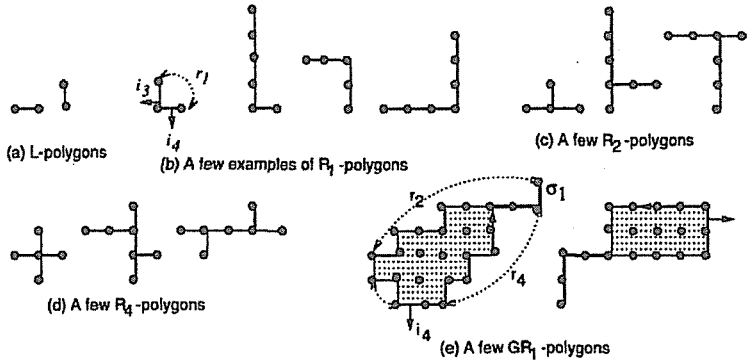


A few sets of indecomposable WTC polygons.

**Proposition 8** *Any WTC polygon resulting from a 2 point binary image is indecomposable.*

**Definition 2** ($R_1$**-polygon**) A WTC polygon is called a $R_1$-polygon if it has the following characteristics: (i) it has only one r-edge, (ii) the multiplicity of that r-edge is 1, and, (iii) both the i-edges adjacent to that non-zero r-edge have lengths 0.

This class of WTC polygons are like simple triangles in the WTC domain.

**Proposition 9** *Every $R_1$-polygon is indecomposable.*

Consider a class of WTC polygons having the following characteristics: (i) the multiplicity of every r-edge in a polygon is 1, and (ii) both the i-edges adjacent to a non- zero r-edge have lengths O. This class can be subdivided into three sub-classes:

1. *$R_1$-polygons (one r-edge):* $(0, z_1, 0, 0, \sigma_3, 0, \sigma_4, 0)$, and affine versions of it.
2. *$R_2$-polygons (two r-edges):* $(0, z_1, 0, z_2, 0, 0, \sigma_4, 0)$, and affine versions of it.
3. *$R_4$-polygons (four r-edges):* $(0, z_1, 0, z_2, 0, z_3, 0, z_4)$, and affine versions of it.

No *$R_3$-polygon*, that is, WTC polygon having three such r-edges can exist physically. $R_1-, R_2-$ and $R_4$-classes of polygons can be considered to be the basic indecomposable classes in the WTC domain.

**Proposition 10** *If every r-edge of a WTC polygon has multiplicity 1 and, both the i-edlges adjacent to every nonzero r-edge have lengths 0, then the polygon is indecomposable.*

**Definition 3** ($GR_1$**-polygon**) A WTC polygon formed by glueing a $R_1$-polygon to another polygon is called, a $GR_1$-polygon.

A typical $GR_1$-polygon $S$ can be expressed as,

$$\partial S = (\sigma_1, 0, 0, [(\sigma_1, \delta_1), \ldots], \sigma_3, z_3, \sigma_4, z_4).$$

**Proposition 11** *Every $GR_1$-polygon is ind,ecomposable.*

The simplest primality test is the trial d,ivision. The simplest indecomposability test would be to take a point set $B$ and check whether $B$ can be a summand of $S$ or not.

**Proposition 12** *A point set $B$ is a summand, of a point set $S$ iff*

$$(S \ominus B) \oplus B = S$$

**Definition 4** (**less than or equal to**) Let $L_1$ and $L_2$ be two taxicab line segments. We say that $L_1$ is *"less than or equal to"* $L_2$ if there exists a taxicab line segment $L_x$, such that $L_2$ can be generated by Minkowski addition of $L_1$ and $L_2$. If $L_x$ turns out to be a single point, we say that $L_1$ is *"equal to"* $L_2$.

This definition matches with our conventional definition of "less than or equal to"

**Proposition 13** *A WTC polygon $B$ cannot be a sum- mand of a WTC polygon $S$ if every $i_j$-edge and, $r_j$-edge of $B$ is not less than or equal to the corresponding $i_j$-edge and $r_j$-edge of $S$.*

Note the resemblance between this proposition and the corresponding proposition regarding convex polygons.

# 5 Brief summing up

Identification of the WTC domain was presented first. Then, efficient algorithms for Minkowski addition and decomposition of binary images were given. Importance of the indecomposability problem in morphology is an importnant issue. We Explored the indecomposability question in a purely number theoretic way.

# Sapporo Guest House Symposium on Mathematics 6

## コンピュータービジョンと微分方程式
## (Computer Vision and Differential Equations)

代表者　後藤 俊一 (金沢大/北大)
儀我 美一 (北大)

２０００年１０月２１日（土）

9:30-10:10　出口 光一郎（東北大・情報）
画像の生成モデル

10:20-11:10　岡谷 貴之（東北大・情報）
画像陰影からの対象の３次元形状回復における諸問題について

11:30-12:20　本谷 秀堅（東大・工）
輪郭線図形の形状解析・記述について

14:30-15:30　池田 勉（龍谷大・理工）
ある非線形放物型方程式の整合差分近似の画像処理への応用

15:40-16:20　上山 英三 (理化学研究所)
不連続を含む時変なベクトル場の推定

16:30-17:10　儀我 美一 (北大・理)
題 未定

札幌天神山ゲストハウス，札幌市豊平区平岸２条１７丁目 1-80
TEL: (011)823-1000　FAX: (011)823-1867

連絡先：儀我　美一
TEL/FAX 011-706-2672
e-mail gjr@math.sci.hokudai.ac.jp

＊参加される方で旅費を必要とされる場合は上記連絡先にその旨ご連絡下さい.

as of November 2, 2001

# Sapporo Guest House Symposium on Mathematics 11

## Image Processing and Differential Equations

Organizers: K. Deguchi (Tohoku U.)
Y. Giga (Hokkaido Univ.)
S. Osher (UCLA)

November 8, 2001 (Thursday)

10:00–11:00 A. Bruckstein (Technion, Israel)
Laplacian Snakes

11:30–12:30 T. Yabe (Tokyo Inst. Tech.)
CIP as a Universal Solver for Solid, Liquid and Gas
– Toward Supra-Real Animation System –

14:30–15:30 R. Kobayashi (Hokkaido U.)
Modeling of Grain Structure Evolution and Singular Diffusivity

16:00–17:00 Y. Giga (Hokkaido U.)
Very Strong Diffusion

18:00–20:00 Welcome Party

November 9, 2001 (Friday)

10:00–11:00 H. Hontani (Yamagata U.)
Contour Shape Analysis and Description using PDE

11:30–12:30 K. Kanatani (Okayama U.)
Fast Display of Curves and Surfaces with Correct Topology

14:30–15:30 J. Sato (Nagoya Inst. Tech.)
Affine Prolongation, Quasi-Invariance and Visual Symmetry

16:00–17:00 R. Kimmel (Technion, Israel)
Applications of Fast Marching on Curved Domains

The venue of symposium:
Sapporo Guest House, 8 minutes walk from Sumikawa (Subway Station)
(札幌天神山ゲストハウス，札幌市豊平区平岸２条１７丁目 1-80)
TEL (011)823-1000 FAX (011)823-1867

連絡先： 儀我 美一 (Y. Giga) TEL/FAX: 011-706-2672
e-mail: gjr@math.sci.hokudai.ac.jp

as of November 7, 2002

# Minisymposium on 'Mathematical Aspects of Image Processing and Computer Vision'

Organizers: Y. Giga (Hokkaido U.)
S. Izumiya (Hokkaido U.)
K. Deguchi (Tohoku U.)

December 6, (Friday)

10:00–11:00 Gilles AUBERT (U. Nice)
Relaxed Problem in Image Analysis

11:30–12:30 Takahiro SHIOTA (塩田隆比呂)(Kyoto U.)
Nonlinear Image Smoothing with Edge and Corner Enhancement

14:45–15:45 Hidekata HONTANI (本谷秀堅)(Yamagata U.)
A Contour Figure Analysis Using a Crystalline Flow

16:20–17:20 Joachim RIEGER (U. Halle, Germany)
Canny Edges and Hypersurfaces of Extremal Slope

18:00– Welcome Party

Venue : Room 3- 508 (Fifth floor of buiding ♯3, Faculty of Science)
Department of Mathematics, Hokkaido University Sapporo 060-0810 Japan.

Correspondence:Y. Giga, TEL/FAX:011-706-2672
e-mail:gjr@math.sci.hokudai.ac.jp